MESHLESS DYNAMIC RELAXATION TECHNIQUES FOR SIMULATING ATOMIC STRUCTURES OF MATERIALS

MESHLESS DYNAMIC RELAXATION TECHNIQUES FOR SIMULATION ATOMIC STRUCTURES OF MATERIALS

By

LI PAN, B.ENG.

A Thesis

Submitted to the School of Graduate Studies

In Partial Fulfillment of the Requirements

For the Degree

Master of Applied Science

McMaster University

MASTER OF APPLIED SCIENCE (2002) McMaster University
(Mechanical Engineering) Hamilton, Ontario

TITLE: Meshless Dynamic Relaxation Techniques for Simulating Atomic Structures of Materials

AUTHOR: Li PAN, B.ENG. (SUES, Shanghai, P. R. China)

SUPERVISOR: Dr. D. R. Metzger, Associate Professor
Department of Mechanical Engineering

Dr. M. Niewczas, Assistant Professor
Department of Materials Science and Engineering

NUMBER OF PAGES: xv, 110

ACKNOWLEDGEMENTS

First of all, the author expresses his deepest gratitude to his two supervisors, Dr. Metzger and Dr. Niewczas, for their patient instruction and valuable advice in this research. Also, the author highly appreciate that they gave the opportunity and provided funding to him to take on this project since he thinks opportunity is the most important thing for a young man. Meanwhile, the author thanks Ms. Rebecca Clifford for her great help for admission in this master program.

Secondly, the author is grateful to his colleagues, Mr. Yihai Shi and Mr. Young Suk Kim. He gets a lot of useful information and advice by many interesting discussions with them.

Thirdly, the author would like to thank his best friend and roommate here, Mr. Wenjiang Wu, for his assistance and jokes throughout the course of this research. Also, appreciation is extended to all his other friends in China and Canada, who give him help and encouragement.

Finally, the author would like to sincerely appreciate his parents, who always support him no matter success or fail. Also, the author thanks his aunt and uncle for their considerations during his study period.

ABSTRACT

Traditionally, Molecular Dynamics combined with pair potential functions or the Embedded Atom Method (EAM) is applied to simulate the motion of atoms. When a defect is generated in the crystalline lattice, the equilibrium of atoms around it is destroyed. The atoms move to find a new place where the potential energy in the system is minimum, which could result in a change of the local atomic structure. This thesis introduces a new Dynamic Relaxation algorithm, which is based on explicit Finite Element Analysis, and pair or EAM potential function, to find equilibrium positions of the block of atoms containing different structural defects.

The internal force and stiffness at the atoms (nodes) are obtained by the first and second derivatives of the potential energy functions. The convergence criterion is based on the Euclidean norm of internal force being close to zero when the potential energy is minimum. The damping ratio affects the solution path so that different damping ratios could lead to different minimum potential energy and equilibrium shapes. The choice of scaled mass of atoms, proper time step, boundary conditions and damping appropriate for the efficient and stable simulation is studied.

A small block of atoms is used to obtain the numerical responses from a hybrid algorithm of potential energy functions and Dynamic Relaxation techniques such as repulsion and attraction in pair potential, minimum configuration, damping effects and different boundary conditions.

The simulation using modified Dynamic Relaxation techniques is performed to the real material model with dislocation defect. The results after relaxation are in agreement with the prediction and current Molecular Dynamics simulation. Therefore, Dynamic Relaxation could be an alternative tool for atomistic simulation.

TABLE OF CONTENTS

LIST OF TABLES

LIST OF FIGURES

0-OUTLINE OF THE THESIS

This thesis consists of five chapters:

The first chapter introduces the basic techniques which have been used in the atomistic simulation. Potential energy functions and numerical methods are discussed. Dynamic Relaxation (DR), being a powerful tool to deal with non-linear problem, is chosen for a new approach to atomistic simulation. The objective of the thesis is included at the end of this chapter.

Since the existing Dynamic Relaxation techniques focus on the structure and continuum problems, Chapter two discusses the development of the Dynamic Relaxation algorithm adapted for atomistic simulation. In the new approach, internal forces and stiffness are defined directly from derivatives of potential energy function. The method of scaling mass is chosen for the simulation. Damping factor and convergence criterion are also addressed here. In addition, several types of boundary conditions are introduced and implemented in the modified DR algorithm.

In order to study the numerical responses after applying the new developed algorithm, in the chapter three, some small fictitious material models are generated to examine various cases. A one-dimensional model is used to show the effect of an attractive and repulsive force, fixed and changing mass algorithm. A two-dimensional model is used to illustrate global minimum potential energy configuration and the effects of applying different boundary conditions. A three-dimensional parallel-atom model is

used to explain the damping ratio effects. Last, a three-dimensional face-central-cubic model is used to present the effects of boundary conditions and a 'defect' of the EAM potential function.

Chapter four gives an example of using modified Dynamic Relaxation to simulate relaxation of a three-dimensional face-centered-cubic lattice with dislocation. Meanwhile, comparison with other existing software is done to verify the validity of this new approach.

Finally, in chapter five, the main conclusions of the thesis are provided as well as the recommendations for the future research work.

CHAPTER 1 – INTRODUCTION

1.1 Introduction to simulating atomistic structures of materials

Computer simulations are increasingly important as a supplement to theory and experiment in material science and engineering. Before computer simulation became practical and popular, making use of a theory that provided an approximate description of that material was the only way to predict the properties of a molecular substance. Such approximations eliminate the complexities which exist in real problems so that they are precise, but only for very few systems for which the equilibrium properties can be solved exactly. As a result, a theoretical model could be easily tested only in few simple special circumstances. If sufficient information about the intermolecular interaction is given, these theories will provide an estimate of the properties of interest. However, the knowledge of the intermolecular interactions is limited to some of the simplest molecules. This leads to a problem if testing the validity of a particular theory by comparing directly to experiment. If the theory and experiment disagree, it may mean the theory is wrong, or there may be some errors or wrong measurement methods in the experiment, or both.

The development of computer simulation techniques altered the traditional relationship between theory and experiment. On the one side, computer simulations increased the demand for accuracy of the models. Some theoretical models that were

difficult to test in the past now are practical to examine. This in turn discloses some critical areas and provides suggestions to improve the models. On the other side, simulation usually can be set close to experimental conditions, to the extent that results of computer simulation can sometimes be compared directly with those of experiments. When this happens, computer simulation becomes an extremely important tool not only to understand and interpret the experiments at the atomic level, but also to study regions which are not accessible experimentally, or which would implement very expensive experiments, such as those involving extremely high pressures or low temperatures.[1][2]

Since computer speeds continue to increase, the atomistic simulation is becoming increasingly common in materials science, and simulations are being designed that more and more closely approximate real materials systems and processes. When a certain defect is generated in the material, the equilibrium of atoms around it is destroyed. The atoms move to find a new place where the potential energy in the system is minimum, which could result in a change of the local atomic structure. Such changes could affect some properties of certain materials. The computers available today allow one to solve tens of millions degrees of freedom and model many material properties, especially equilibrium properties. The results after simulation then could be used to control the material behaviour for the manufacturing purpose.

1.2 Potential energy functions

Movement of the atoms is dependent on the potential energy. The key factor in making a connection between simulation and reality is the accuracy of the atomic model

for the interatomic forces, which are derived from a potential function. The properties predicted by an atomistic simulation are only as good as the quality of the interatomic potential energy. Usually, the pair potential and embedded-atom method are widely used as the interatomic potential functions.

1.2.1 Pair potential energy functions (Lennard-Jones potential)

Since a direct determination of potential function $V(r_{ij})$, which is between two atoms i and j separated by a distance r, is very difficult either experimentally or theoretically, it is common to use model potentials. Some basic requirements must be satisfied for the model potential to be physically acceptable: (i) the lattice is symmetric; (ii) rigid body translations and rotations are invariant; (iii) the lattice is stable. Moreover, the model potential needs to consider the correct value of physically observed quantities like third order elastic constants, formation and activation energies of defects etc.[3] In the case of metals, it is important to consider the effect of free electrons.

The potential function in the form of a pair potential is the simplest approach to constructing the model potentials. This model potential does not explicitly account for the electron gas. The parameters of the pair potential can be determined by using the measured values of some physical properties of solid, in which case the parameters are expected to account for the electron gas in an effective manner. Alternatively, the pair potential is assumed to represent that part of the potential which is independent of the free electrons. The contribution of the free electrons can be treated as a volume-

dependent term to be added to the pair potential energy function separately. The most common potential functions are the following[3]:

(i) Born-Mayer potential

$$V(r_{ij}) = A\exp[-\rho(r_{ij} - r_o)/r_o] \tag{1.1}$$

where A and ρ are arbitrary constants and r_o is the equilibrium nearest neighbour distance.

(ii) Morse potential

$$V(r_{ij}) = A\exp[-2\rho(r_{ij} - r_o)] - 2A\exp[-\rho(r_{ij} - r_o)] \tag{1.2}$$

(iii) Lennard-Jones potential (12-6)

$$V(r_{ij}) = 4\varepsilon\left[\left(\frac{\sigma}{r_{ij}}\right)^{12} - \left(\frac{\sigma}{r_{ij}}\right)^{6}\right] \tag{1.3}$$

where the parameter σ and ε are chosen to fit the physical properties of the material. The pair potential method is an empirical approach, which has no theoretical foundation.

The Lennard-Jones 12-6 pair potential energy function is an extremely important model potential. There are numerous papers which have investigated the behaviour of atoms interaction via Lennard-Jones pair potential for a variety of different geometries (solid, surfaces, clusters, etc) so that the Lennard-Jones potential becomes the standard potential to investigate fundamental issues, rather than studying the properties of a specific material.[2]

The Lennard-Jones pair potential is a function of distance r_{ij}. The balance distance is around 1.122σ, and the repulsive force is stronger at shorter distances, passing through 0 at $r = \sigma$ and increasing steeply as r is decreased further. The term $\sim 1/r^{12}$ dominates at short distance and models the repulsion between atoms when their positions are very close to each other. As explained in [2], its physical origin is related to the Pauli principle: when the electronic clouds surrounding the atoms start to overlap, the energy of the system increases abruptly. The exponent 12 was determined based on the practical criterion that equation (1.3) is particularly easy to compute. However, on the physical side, the exponential function behaviour would be more appropriate.[2]

The term $\sim 1/r^6$ dominates at large distance and constitutes the attractive part. This is the term which gives cohesion to the system. A $1/r^6$ attraction comes from Van Der Waals dispersion forces and dipole-dipole interactions in turn due to fluctuating dipoles. These are rather weak interactions. However they dominate the bonding character of closed-shell systems, that is, rare gases materials such as Ar or Kr, for which a Lennard-Jones potential is fairly accurate.[2]

When using the Lennard-Jones pair potential in simulation, it is usual to work in a system of units where $\sigma = 1$ and $\varepsilon = 1$. Then the equation (1.3) is changed to

$$V(r_{ij}) = 4\left[\left(\frac{1}{r_{ij}}\right)^{12} - \left(\frac{1}{r_{ij}}\right)^{6}\right] \tag{1.4}$$

By summing the potentials for all pair sets in a system, the total potential energy of the system using pair potential energy function is

$$U_{tot} = \frac{1}{2}\sum_{i,j} V(r_{ij}) \tag{1.5}$$

The Lennard-Jones pair potential is not suitable to all the material models. In some systems, like those with strong localized bonds which may form in covalent system, or if there is a delocalised "electron sea", such as when ions sit in metals, the two-body interactions scheme itself is not successful.[2]

1.2.2 Embedded Atom Method functions (FS EAM potential)

Although the pair potential is successful in many cases, while applied to metals, the pair potential model has two main drawbacks:

(i) It does not properly reproduce elastic constants;

(ii) It largely overestimates formation energy for different internal defects presented in the material.

Because of the above, over the past two decades, researchers focused on generating new potential functions to get more realistic results. This new approach was proposed by Daw and Baskes[4] and is called the embedded-atom method (EAM). In this scheme, the energy of an atom i (U_i) is written as

$$U_i = -f(\rho_i) + \frac{1}{2}\sum_j V(r_{ij}) \tag{1.6}$$

and the total energy of the system is

$$U_{tot} = \sum U_i \tag{1.7}$$

Here $V(r_{ij})$ is a central pair potential, $f(\rho_i)$ is an embedding function and

$$\rho_i = \sum_j \phi(r_{ij}) \tag{1.8}$$

where $\phi(r_{ij})$ is the pairwise interaction between atoms and ρ_i is an electron gas density term. The sums over neighbour atoms (j) are limited by the range of the cut-off distance for ϕ and ρ, which is generally from one to four nearest neighbours in the perfect crystal. The computational procedure for calculating the EAM potential energy is similar to that for a pair potential. For atom i, both $\phi(r_{ij})$ and $\rho(r_{ij})$ are summed over neighbours j within the cut-off distance, and then a single evaluation of $f(\rho_i)$ is performed.[5]

The values of ρ_i represent a measure of the atomic density in the neighbourhood of atom i, which, in turn, requires that function $\rho(r_{ij})$ be a monotonically decreasing function of r_{ij}. Therefore, the EAM potential energy function can be thought as the generalization of the fixed-volume pair potentials.[6] Here the 'volume' is now defined for each atom rather than the whole system. Since ρ_i depends only on scalar distances to neighbouring atoms, the many-body term has no angular dependence.[5]

The key point to EAM is the nonlinearity of the function $f(\rho_i)$. If $f(\rho_i)$ were purely linear, the two terms in equation (1.6) could be transformed to give a simple pair potential. A nonlinear $f(\rho_i)$ thus provides a many-body contribution to the potential

energy function.[5] Many researchers then focus on how to generate the function $f(\rho_i)$ to make EAM perform well. For example, Finnis and Sinclair (to be referred to as FS)[7] presented a simple scheme for deriving an empirical N-body interatomic potential for metallic systems. They used a square-root function for $f(\rho_i)$ to mimic the result of tight-binding theory in which $\phi(r_{ij})$ would be interpreted as a sum of squares of overlap integrals[8]. Kogure and Kosugi[9] also developed a new format for $f(\rho_i)$:

$$f(\rho_i) = D\rho_i \ln \rho_i \tag{1.9}$$

where D is determined by fitting the functions to the experimental values of the cohesive energy E_c, the lattice parameter a, the material stiffness (C_{11}, C_{12}, C_{44}) and the formation energy of the vacancy E_V.

Ackland *et al*[10] gave the formula for simple N-body potentials of the FS type for the face-centred- cubic (f.c.c.) noble metals and nickel.

$$V(r_{ij}) = \sum_{k=1}^{6} a_k (r_k - r_{ij})^3 H(r_k - r_{ij}) \tag{1.10}$$

$$\phi(r_{ij}) = \sum_{k=1}^{2} A_k (R_k - r_{ij})^3 H(R_k - r_{ij}) \tag{1.11}$$

where r_k and R_k are chosen knot points such that $r_1 > r_2 > r_3 > r_4 > r_5 > r_6$ and $R_1 > R_2$. $H(x) = 0$ for $x < 0$ and $H(x) = 1$ for $x > 0$. Hence, r_1 and R_1 represent the cut-off

distances of function $V(r_{ij})$ and $\phi(r_{ij})$, respectively. For most cases, these distances were set to the radius of the third-nearest neighbouring atom in the perfect volume f.c.c. lattice. r_6 was set equal to the nearest-neighbour spacing r_{nn} in all cases, so that the term multiplied by a_6 contributes only for $r < r_{nn}$ where the pair potential is strongly repulsive. The coefficient a_1, ..., a_5, A_1 and A_2 have been determined by fitting exactly to the equilibrium f.c.c. lattice parameter a, the cohesive E_c, the material stiffness C_{11}, C_{12}, C_{44}, a lower bound of the unrelaxed vacancy formation energy E_V^f and the stacking fault energy. The coefficient a_6 cannot be found by fitting to any harmonic property of the ideal lattice, so it was then adjusted for metals, like copper, so as to fit the pressure-volume relation calculated by Christensen and Heine[11] using self-consistent band structure calculations.[10] Since the test material in the thesis is copper, the parameters of it are summarized in table 1.1.

In short, EAM provides more accuracy than pair potential methods and offers more reasonable interpretation for the phenomena in material science area. But EAM needs much more computer calculation time than simple pair potential, like the Lennard-Jones potential, which causes a problem when the number of atoms is very large. Until today, EAM is continuing to be developed to be more accurate and efficient.

Coefficient	Copper
a_1	29.059214
a_2	-140.05681
a_3	130.07331
a_4	-17.48135
a_5	31.82546
a_6	71.58749
R_1	1.2247449
R_2	1.0000000
A_1	9.806694
A_2	16.774638
r_1	1.2247449
r_2	1.1547054
r_3	1.1180065
r_4	1.0000000
r_5	0.8660254
r_6	0.7071068
The lattice parameter $a = 3.615$ Å	

Table 1.1 Fitting coefficients for copper
(The coefficients for V and ϕ are in electron volts and values of r_k and R_k are in units of the lattice parameter.)
(from Ackland *et al.* , 1987)

1.3 Developed numerical methods for atomistic simulation

Numerical methods are used in the implementation for computers to calculate the change of the local atomic structure after relaxation. Since the atomic model is a highly non-linear system, the specification of numerical methods should be made to maintain the stability of the global atomic structure. Any inappropriate numerical operations could

make system become unstable or break the model into several parts. So far, two types of numerical method are popular to do the atomistic simulation. They are the Monte Carlo method and the Molecular Dynamics method.

1.3.1 Monte Carlo Method

Any Monte Carlo technique is a statistical mechanics simulation method. The statistical simulation can be defined as a method that uses sequences of random numbers to perform the simulation. For the past several decades, Monte Carlo methods have been developed rapidly to become a powerful method to solve most complex applications, which includes atomistic simulation.

The fundamental idea of Monte Carlo methods is different from regular numerical discretization methods, e.g. finite element method, which describe physical or mathematical system behaviour using ordinary or partial differential equations, discretize the differential equations and then solve a list of algebraic equations for the unknown state of the system. In a Monte Carlo method, the simulation for the physical process is direct. The physical or mathematical system is described by probability density functions (pdf) rather than the differential equations. Once the pdf are known, the Monte Carlo method uses random sampling techniques to sample from these pdf, which necessitates a fast and effective way to generate random numbers uniformly distributed on the interval [0,1]. The results of these random samplings should be accumulated or tallied in an appropriate manner to produce the desired solution of physical problem.[12]

In atomistic simulations, the brief scheme using Monte Carlo method from Metropolis *et al.* is as follows[1]:

(1) From current positions of one atom, calculate its potential energy via pair potential energy function or EAM function.

(2) Give the atom random displacements based on certain rules, and calculate its new potential energy.

(3) Accept the above movement from old position to new position with certain probability function based on old potential energy and new potential energy. If rejected, the old configuration is retained.

(4) Repeat procedure (1) to (3) in reasonable cycles to get final result.

We can predict the statistical error in the average result, so it is possible to estimate the number of Monte Carlo trials in atomistic simulation needed to achieve a given error.

A Monte Carlo method could apply to real or non-real physical process because it is direct to the pdf of the system. Therefore, This method is suitable to a wide range of areas, but it may consume more computational time.

1.3.2 Molecular Dynamics method

Molecular Dynamics methods appeared in 1950s. The first paper about Molecular Dynamics was published in 1957 and written by Alder and Wainwright[13]. After that, with the increase of computer speed, Molecular Dynamics was developed to deal with more atoms and various applications. Nowadays, Molecular Dynamics has become a standard computer tool to simulate the movement of atoms.

In Molecular Dynamics, classical mechanics or Newton's law is used. For each atom i in a system,

$$\mathbf{F}_i = m_i \mathbf{a}_i \tag{1.12}$$

Here m_i is the atom mass; $\mathbf{a}_i$ is its acceleration; and $\mathbf{F}_i$ is the force acting on it due to interactions with other atoms. Therefore, Molecular Dynamics is a deterministic method compared to the Monte Carlo method. Given initial positions and velocities to the system, the subsequent time evolution is determined. However, Molecular Dynamics could be still regarded as a statistical mechanics method somewhat because the initial condition is determined according to some statistical distribution function.[2]

The scheme of atomistic simulation using a Molecular Dynamics technique is as follows[1]:

(1) Get the parameters from specific conditions for a certain system, e.g., initial temperature, number of atoms, time step and so on.

(2) Initialize the system: (i) select initial positions of atoms according to the lattice type. (ii) give random velocities to every atom using certain statistical distribution function.

(3) Compute the forces on all atoms from pair potential energy function or EAM potential energy function.

(4) Integrate Newton's equations of motion to get the new positions of atoms. This part is the core of the simulation. Usually, a conjugate gradient algorithm[14] or the Verlet algorithm[1] is applied here. The procedure (3) and (4) is repeated until the properties of the system no longer change with time (practically, the

simulation is terminated after the running time exceeds pre-set maximum time.)

After completion of above simulation procedures, various physical quantities, such as the temperature, the energy of the system or Burger's vector of dislocation in relaxed lattice, can be determined.

The Molecular Dynamics simulation is a technique to compute the equilibrium and transport properties using classical mechanics, which is an excellent approximation for a wide range of materials. However, when simulating light atoms or molecules (He, H_2), quantum effects should be considered.[1]

1.4 Dynamic Relaxation techniques

As mentioned above, both Monte Carlo method and Molecular Dynamics technique obey the classical mechanics and are based on certain statistical functions. Therefore, as an alternative, a pure mechanics technique without any statistical functions could be possible to simulate the motion of atoms. The new approach is Dynamic Relaxation (DR) technique in Finite Element Methods (FEM).

1.4.1 Overview

The basic idea of using Finite Element Methods to do the atomistic simulation comes from direct impression that Finite Element mesh and crystal lattice in materials, e.g. metals, are very similar. Figure 1.1 and Figure 1.2 show the Finite Element 3D mesh and lattice with screw dislocation in materials respectively. If atoms are looked at as nodes in a Finite Element method, the two models are close to being the same.

Having been developed for more than half century, Finite Element methods are now powerful and popular numerical discretization methods for many different areas of mechanics and physics. The basic scheme of the Finite Element method is following[15]:

(i) The model is discretized by a series of finite elements;

(ii) Each element has simple properties compared to the whole model so that algebraic equation rather than differential equation could describe it. That is, the governing differential equation for the whole model is discretized by a list of algebraic equations from elements.

(iii) These algebraic equations are solved in a self-consistent manner by a certain numerical method to get the approximate results for the whole model. The material model could be viewed as being discretized by atoms automatically.

The Finite Element method determines the displacements of nodes after certain loads are applied to the model. From the displacements, other properties, e.g. stress field, can be derived. Also, the main purpose for atomistic simulation here is to study the movement of atoms during non-equilibrium state of certain material. Therefore, the Finite Element method, as a mature tool, is suitable to atomistic simulation as well.

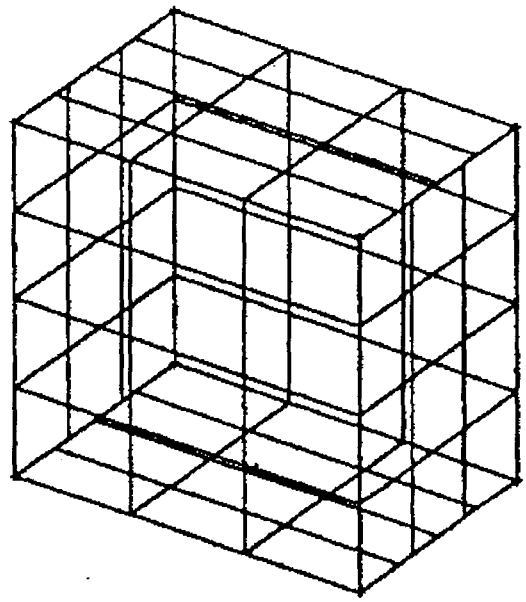

Figure 1.1 Finite Element 3D mesh

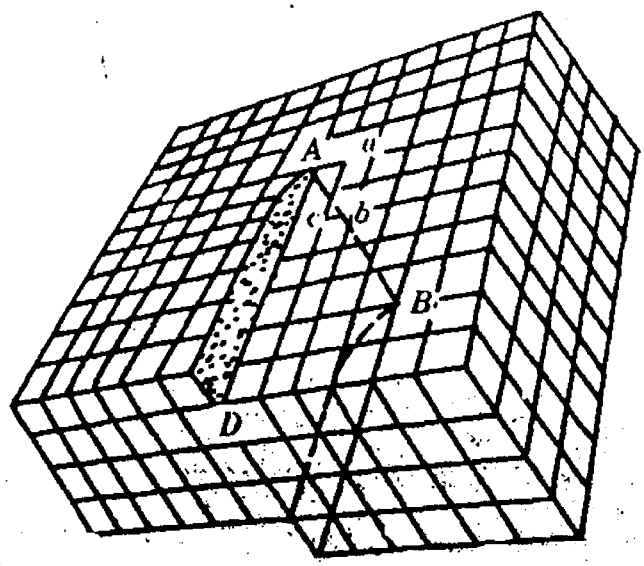

Figure 1.2 Material lattice with screw dislocation

1.4.2 Background

It is a typical steady-state problem that atoms in one equilibrium state (perfect lattice) move to another equilibrium state when a disturbance is applied (relaxation for certain defect). The Dynamic Relaxation technique is a very good method which can be used with Finite Elements to solve steady-state problems.

Dynamic Relaxation techniques appeared in 1960s[16] for the solution of finite difference approximations to the partial differential equations. Meanwhile, Dynamic Relaxation can be efficiently implemented into the Finite Element method. Some previous papers, e.g. Brew and Brotton[17], and, Pica and Hinton[18] described how to use Dynamic Relaxation and in the same time allowed overshoot for the solution. Although overshoot is not a severe limitation for problems of linear nature, it is not acceptable for nonlinear problem such as elastic-plastic materials problem whose responses are history-dependent (path dependent). Kant and Patel[19] in 1990 introduced a Dynamic Relaxation method for solving nonlinear structure problems, but the method still encountered overshoot problems. Thus it was only suitable for small deformation and linear materials. In Underwood's paper[20], adaptive damping, mass and time step were derived, which leads to the critically damped steady-state solution for an applied loading (presumably without overshoot). Following his ideas, Sauvé and Metzger[21] in 1995 suggested an algorithm for Dynamic Relaxation which is applicable to highly nonlinear problems without overshoot and compatible with the Finite Element method.

Thus, there are three benefits from Dynamic Relaxation to do atomistic simulations:

(i) Dynamic Relaxation deals with nonlinear problem very well. The material model

under either pair potential function or EAM function is highly nonlinear system.

(ii) Usually, several thousands of 3D atoms are needed in the atomistic simulation. Dynamic Relaxation uses explicit central difference operator so that large computer storage is not necessary. Therefore, tens of thousands of degrees of freedom is possible in the calculation.

(iii) It is a history dependent problem, which means that current positions of atoms (potential energy) directly affect the motion of atoms in the next time step. Overshoot in the atomistic simulation leads to improper movement of atoms, which could result in failure to keep the global shape of the model. Present Dynamic Relaxation algorithms can avoid or control overshoot for history dependent problems in the simulation. Therefore, this is an advantage to use Dynamic Relaxation for atomistic simulations.

1.4.3 Analysis

Since Dynamic Relaxation shows its strong potential for atomistic simulation as discussed in chapter 1.4.2, here a brief introduction is provided to the principle and algorithm of Dynamic Relaxation, according to the paper by Sauvé and Metzger[21].

(a) Explicit central difference operator

The explicit central difference operator is a numerical method for the time integration of the discretized equations of motion

$$M\ddot{\mathbf{x}} + \mathbf{F}_{\text{int}}^{t} = \mathbf{F}_{ext}^{t} \tag{1.13}$$

where M is the mass matrix, $\mathbf{F}_{\text{int}}^{t}$ and $\mathbf{F}_{ext}^{t}$ are internal and external force vectors, respectively. The complete presentation of the central difference method was given by Belytschko[22] in 1983. Here is a brief description of the topic.

Accelerations $\ddot{\mathbf{x}}$, velocities $\dot{\mathbf{x}}$ and coordinates/displacements $\mathbf{x}$ are known at time $\mathbf{t}$ in one system. In order to obtain above quantities at the next time $t + \Delta t$, where Δt is a time increment, from Equation (1.13), the acceleration $\ddot{\mathbf{x}}^{t}$ is calculated as

$$\ddot{\mathbf{x}}^{t} = M^{-1}(\mathbf{F}_{ext}^{t} - \mathbf{F}_{\text{int}}^{t}) \tag{1.14}$$

The new velocities are described as

$$\dot{\mathbf{x}}^{t+\Delta t/2} = \dot{\mathbf{x}}^{t-\Delta t/2} + \Delta t\ddot{\mathbf{x}}^{t} \tag{1.15}$$

The superscript $t + \Delta t/2$ means $\dot{\mathbf{x}}^{t+\Delta t/2}$ is a half-step approximation. This velocity value is thought to be constant as configuration moves from time t to time $t + \Delta t$. The new coordinates of the system then become

$$\mathbf{x}^{t+\Delta t} = \mathbf{x}^{t} + \Delta t\dot{\mathbf{x}}^{t+\Delta t/2} \tag{1.16}$$

From this new configuration, strains are interpolated and the stresses are obtained by appropriate constitutive laws. The internal forces then could be evaluated element by element.

$$\mathbf{F}_{\text{int}}^{t+\Delta t} = \int_{V} \mathbf{B}^{\mathrm{T}} \sigma \, \mathrm{dV} \tag{1.17}$$

Here $\mathbf{B}$ is a matrix relating element nodal velocities to interpolated element strain rates and σ is stress field in the element. Then, the new accelerations are calculated by external forces and updated internal forces.

At each time step, all constitutive calculations and element geometry are evaluated in an updated configuration frame defined by current coordinates, $\mathbf{x}^{t+\Delta t}$. The mass matrix, M, is transformed to lumped (diagonal) mass matrix to decouple the system easily. This allows equation (1.14) to be solved without the need to factor a full matrix.

The above time integration is defined as explicit in that all the unknown quantities such as $\mathbf{x}^{t+\Delta t}$ are determined based on completely historical information. Thus, the computer memory requirement for explicit method is small. However, the explicit operator is conditionally stable. The time step Δt must be lower than a critical time step, which is based on the Courant limit:

$$\Delta t_{cr} \leq \frac{2}{\omega_{\max}} \tag{1.18}$$

where $\omega_{\max}$ is the highest frequency of the system[22].

The above operator has a stable time step that is as large as most explicit methods and needs no special starting scheme. Furthermore, the overall implementation of this operator is applicable to both linear and highly nonlinear problems.

(b) Dynamic Relaxation algorithm

The idea of Dynamic Relaxation is that the solution of a static problem is viewed as the steady-state solution of a damped transient equation. For time t, the governing equation of motion of the system is:

$$M\ddot{\mathbf{x}}^t + C\dot{\mathbf{x}}^t + \mathbf{F}_{\text{int}}(\mathbf{u}^t) = \mathbf{F}_{ext}^t \tag{1.19}$$

Here C is a damping matrix and $\mathbf{u}^t$ is displacement vector. Time t could be referred to an iteration (cycle) counter. For nonlinear problems, as mentioned in chapter 1.4.3 (a). $\mathbf{F}^t_{\text{int}}(\mathbf{u}^t)$ is used in place of $K(x^t)\mathbf{u}^t$, which avoids complicated calculation for forming $K(x^t)$ at every time step.

From equation (1.15) and (1.16), the central difference operator could be changed to equation (1.20) and (1.21).

$$\ddot{\mathbf{x}}^t = \frac{\dot{\mathbf{x}}^{t+\Delta t/2} - \dot{\mathbf{x}}^{t-\Delta t/2}}{\Delta t} \tag{1.20}$$

$$\dot{\mathbf{x}}^{t+\Delta t/2} = \frac{\mathbf{x}^{t+\Delta t} - \mathbf{x}^t}{\Delta t} \tag{1.21}$$

The average value of velocity for time t is calculated as

$$\dot{\mathbf{x}}^t = \frac{\dot{\mathbf{x}}^{t+\Delta t/2} + \dot{\mathbf{x}}^{t-\Delta t/2}}{2} \tag{1.22}$$

Substituting equation (1.20), (1.21) and (1.22) into equation (1.19) yields

$$M\frac{\dot{\mathbf{x}}^{t+\Delta t/2} - \dot{\mathbf{x}}^{t-\Delta t/2}}{\Delta t} + C\frac{\dot{\mathbf{x}}^{t+\Delta t/2} + \dot{\mathbf{x}}^{t-\Delta t/2}}{2} + \mathbf{F}^t_{\text{int}} = \mathbf{F}^t_{ext} \tag{1.23}$$

which is rearranged to

$$\dot{\mathbf{x}}^{t+\Delta t/2} = \left(\frac{M}{\Delta t} + \frac{C}{2}\right)^{-1} \times \left[\left(\mathbf{F}^t_{ext} - \mathbf{F}^t_{\text{int}}\right) + \left(\frac{M}{\Delta t} - \frac{C}{2}\right)\dot{\mathbf{x}}^{t-\Delta t/2}\right] \tag{1.24}$$

To maintain the efficiency and form of central difference operator, and ensure that the mode associated with the applied loading distribution is critically damped as well, the mass proportional damping is used.

$$C = 2\omega M \tag{1.25}$$

where ω is the undamped natural frequency corresponding to the participating mode of loading. Substituting for C in equation (1.24) yields

$$\dot{\mathbf{x}}^{t+\Delta t/2} = \frac{1-\omega\Delta t}{1+\omega\Delta t}\dot{\mathbf{x}}^{t-\Delta t/2} + \frac{\Delta t M^{-1}(\mathbf{F}_{ext}^{t} - \mathbf{F}_{\text{int}}^{t})}{1+\omega\Delta t} \tag{1.26}$$

Combined with equation (1.14), equation (1.26) now becomes

$$\dot{\mathbf{x}}^{t+\Delta t/2} = \frac{1-\omega\Delta t}{1+\omega\Delta t}\dot{\mathbf{x}}^{t-\Delta t/2} + \frac{\Delta t}{1+\omega\Delta t}\ddot{\mathbf{x}}^{t} \tag{1.27}$$

After equation (1.27), displacement vector is obtained as

$$\mathbf{u}^{t+\Delta t} = \mathbf{u}^{t} + \Delta t\dot{\mathbf{x}}^{t+\Delta t} \tag{1.28}$$

Also, the current coordinates are calculated based on equation (1.16). Thus, the transient responses are attenuated by the damping step-by-step, which results in the steady-state solution,

$$\mathbf{F}_{\text{int}} = \mathbf{F}_{ext} \tag{1.29}$$

In the dynamic relaxation techniques, $\mathbf{F}_{\text{int}}$ and $\mathbf{F}_{ext}$ represent the real system. Since accelerations and velocity of the system are dissipated to zero at the end by the damping,

$\{M\ddot{\mathbf{x}} + C\dot{\mathbf{x}}\}$ are arbitrary dynamic items. Therefore, mass could be scaled to make simulation as fast as possible but it needs to maintain the stability of the central difference operator. The participating frequency ω is dependent on M. Making good choice of the mass matrix could maintain the stability and optimize the rate of convergence as well.

As presented by Underwood[20] (1983), the spectral radius R is an indicator for the convergence rate of dynamic relaxation.

$$R = \left| 1 - 2\left(\frac{\omega}{\omega_{\max}} \right) \right| \tag{1.30}$$

where $\omega_{\max}$ and ω are the highest and lowest frequencies of the discretized numerical model. By maximizing the ratio $\omega / \omega_{\max}$ (minimizing R), the fastest convergence rate is obtained. The highest frequency $\omega_{\max}$ is mesh and material-dependent, while lowest frequency ω is based on the lowest participating mode of structure corresponding to the loading distribution.

The highest frequency of the system $\omega_{\max}$ could be estimated as

$$\omega_{\max} = \frac{2C_D}{L_{\min}} \tag{1.31}$$

Here C_D is the speed of sound of a dilatational wave, and $L_{\min}$ is the minimum effective element length in the problem. The critical time step is then calculated as:

$$\Delta t_{cr} = \frac{L_{\min}}{C_D} \tag{1.32}$$

In the implementation, the density is adjusted for each element (change the mass of every node) to obtain the same time step for each element. Usually, the element densities are set to obtain $\Delta t_{cr} = 1.05$. Then the real time step for Dynamic Relaxation solution is a unit time step ($\Delta t = 1.0$) so that the stability of system is ensured. The densities will be adjusted in the simulation once the critical time step drops below 1.001.

Another important issue for Dynamic Relaxation is to avoid overshoot. Typically, critical damping is applied to the participating frequency ω which tends to begin at a high frequency of the system. Therefore, the lowest participating frequency is overdamped at the current time. With more iterations, the participating frequency ω becomes lower as high frequencies damp out. When the lowest participating frequency is critically damped, high frequencies are underdamped but they are already gone at this time. The solution from this approach will be below the true response so that overshoot doesn't appear.

The Rayleigh quotient is used to obtain an approximation for ω, for cycle t,

$$\omega^t \approx \left[\frac{\left(\mathbf{u}^t\right)^T K \mathbf{u}^t}{\left(\mathbf{u}^t\right)^T M \mathbf{u}^t} \right]^{1/2} \tag{1.33}$$

where $\mathbf{u}$, K and M are current displacement vector, tangent stiffness matrix ($K_{ij} = \frac{\partial \mathbf{F}_{int}}{\partial \mathbf{u}_j}$) and mass matrix, respectively. The superscript T indicates transpose of the matrix.

Since the stiffness is not directly calculated in an explicit method, the estimate of

current tangent stiffness K could be obtained as an approximate diagonal stiffness as

$$K^t \equiv \frac{[\mathbf{F}_{\text{int}}^t - \mathbf{F}_{\text{int}}^{t-\Delta t}]}{\Delta t \dot{\mathbf{x}}^{t-\Delta t/2}} \tag{1.34}$$

Its component can be in form for degree of freedom i,

$$K_{ii}^t \equiv \frac{[\mathbf{F}_{\text{int}\,i}^t - \mathbf{F}_{\text{int}\,i}^{t-\Delta t}]}{\Delta t \dot{\mathbf{x}}_i^{t-\Delta t/2}} \tag{1.35}$$

To avoid possible unstable regions encountered in nonlinear problem, only positive values of ω are admissible, i.e. $\omega = \max(\omega^t, 0)$. Also, use of $\dot{\mathbf{x}}$ for the mode shape in equation (1.33) can simplify ω to be given by

$$\omega = \sqrt{\frac{(\dot{x}^{t-\Delta t/2})^T K \left(\dfrac{u^t - u^{t-\Delta t}}{\Delta t} \right)}{(\dot{x}^{t-\Delta t/2})^T M \dot{x}^{t-\Delta t/2}}} = \sqrt{\frac{\sum_{i=1}^{n} \dot{x}_i^{t-\Delta t/2} (F_{\text{int}}^t - F_{\text{int}}^{t-\Delta t})/\Delta t}{\sum_{i=1}^{n} (\dot{x}_i^{t-\Delta t/2})^2 m_{ii}}} \tag{1.36}$$

This formula is actually used in the Dynamic Relaxation algorithm.

Convergence criteria are chosen to balance the productive cycles and accurate results. Here the following two inequalities are used as convergence criteria:

$$\frac{\left\| \mathbf{F}_{ext}^t - \mathbf{F}_{\text{int}}^t \right\|_2}{\left\| \mathbf{F}_{ext}^t \right\|_2} < f_{tol} \tag{1.37}$$

$$\frac{\left\| \Delta t \dot{\mathbf{x}}^{t+\Delta t/2} \right\|_2}{\left\| \mathbf{u}^{t+\Delta t/2} \right\|_2} < u_{tol} \tag{1.38}$$

where $\| \|_2$ indicates Euclidean norm. f_{tol} and u_{tol} are tolerance numbers for force and displacement, which are chosen before simulation starts. When both criteria are met, the iteration will be terminated.

1.4.4 Summary

The algorithm of Dynamic Relaxation is summarized in table 1.2. It provides an efficient and accurate solution to problems involving varying degrees of nonlinearity. It was easily adapted into existing finite element framework. It has been implemented into a general finite element code and is currently in use on a wide variety of problems in mechanical areas, especially highly nonlinear problems.

Table 1.2 Dynamic Relaxation algorithm
(From Sauvé and Metzger, 1995)

I. Initialize M for $\Delta t_{cr} = 1.05$ for each element, set $\Delta t = 1.0$.

II. At cycle t for load increment i

(i) $\ddot{x}^t = M^{-1}[\mathbf{F}_{ext}^t - \mathbf{F}_{\text{int}}^t]$

(ii) $\dot{\mathbf{x}}^{t+\Delta t/2} = \dfrac{(1-\xi\omega\Delta t)}{(1+\xi\omega\Delta t)}\dot{\mathbf{x}}^{t-\Delta t/2} + \dfrac{\Delta t}{(1+\xi\omega\Delta t)}\ddot{\mathbf{x}}^t$

$$\mathbf{u}^{t+\Delta t} = \mathbf{u}^t + \Delta t\dot{\mathbf{x}}^{t+\Delta t/2}$$

$$\mathbf{x}^{t+\Delta t} = \mathbf{x}^t + \Delta t\dot{\mathbf{x}}^{t+\Delta t/2}$$

(*iii*) Update external force vector $\mathbf{F}_{ext}^{t}$

(*iv*) Check error norms

$$\frac{\left\|\mathbf{F}_{ext}^{t}-\mathbf{F}_{\text{int}}^{t}\right\|_2}{\left\|\mathbf{F}_{ext}^{t}\right\|_2}<f_{tol}\ ;\ \frac{\left\|\Delta t\dot{\mathbf{x}}^{t+\Delta t/2}\right\|_2}{\left\|\mathbf{u}^{t+\Delta t/2}\right\|_2}<u_{tol}$$

If satisfied go to next load increment $i+1$

(*v*) Obtain current internal force vector $\mathbf{F}_{\text{int}}^{t+\Delta t}$ and current stable time step Δt_{cr}

(*vi*) Update density if $\Delta t_{cr}<1.001$

(*vii*) Obtain current estimate of ω

$$K_{ii}^{t}=\dot{\mathbf{x}}^{t+\Delta t/2}(\mathbf{F}_{\text{int}}^{t+\Delta t}-\mathbf{F}_{\text{int}}^{t})/\Delta t$$

$$K_{ii}^{t}=\max(K_{ii}^{t},0)$$

$$\omega=\left[\frac{\sum K_{ii}^{t}}{\sum M_{ii}(\dot{\mathbf{x}}^{t+\Delta t/2})^2}\right]^{1/2}$$

(*vi*) Go to (*i*) and repeat

1.5 Objectives of this thesis

The main objectives of the research are:

(1) Modify the Dynamic Relaxation algorithm to combine with pair potential energy function and EAM potential function, which could adapt to the atomistic simulation.

(2) Study the numerical responses after applying modified Dynamic Relaxation algorithm to the small fictitious material model.

(3) Simulate normal material model with dislocation for practical purposes.

(4) Compare the relaxation results with other existing software to verify the modified Dynamic Relaxation algorithm.

CHAPTER 2 – MODIFIED DYNAMIC RELAXATION ALGORITHM FOR ATOMISTIC SIMULATION

2.1 Background

In Chapter 1, the Dynamic Relaxation technique and the possibility to use this technique for atomistic simulation have been discussed. However, these calculations cannot be carried out directly by the original Dynamic Relaxation algorithm. In this chapter, modifications that are necessary to incorporate into the Dynamic Relaxation algorithm to deal with the atomistic simulation are discussed.

There are two reasons for this:

(i) Interpolation

In regular Finite Element analysis, the approximating displacement field in three dimensions u, v, w of every element is generated by interpolation. Generally, simple polynomials are adequate to describe the displacement field. The terms of interpolated displacement polynomial are related to the element types. That is, the number of nodes in one element is equal to the number of displacement polynomial terms, which is based on Rayleigh-Ritz method. The convergence condition for Rayleigh-Ritz method is that the displacement field be complete. In three dimensions, a polynomial is of degree n if it contains a term of the form $x^l y^m z^p$, where l, m and p are nonnegative integers and

$l+m+p=n$. The complete displacement polynomial requires that it contains all combinations of l, m and p for which $l+m+p=n$ and no lower-order terms are omitted.[15] Practically, there are four types of elements for 3D calculations: constant strain tetrahedron, linear strain tetrahedron, trilinear hexahedron and quadratic hexahedron. (Figure 2.1)

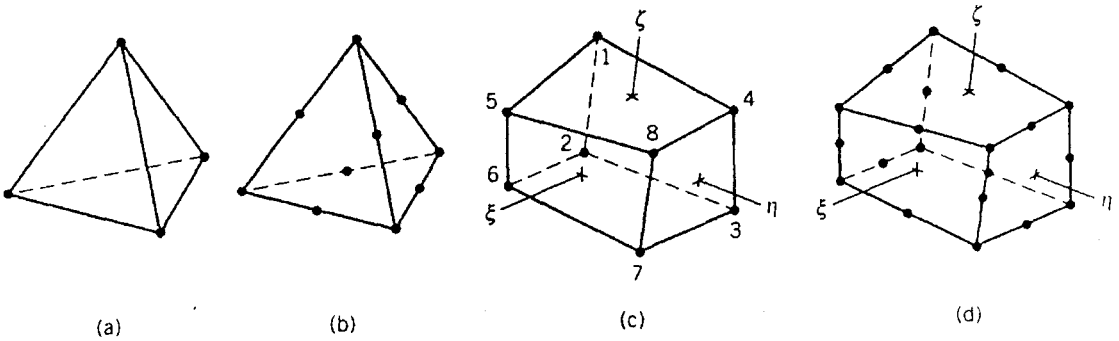

Figure 2.1 (a) Constant strain (four-node) tetrahedron. (b) Linear Strain (ten-node) tetrahedron. (c) Trilinear (eight-node) hexahedron. (d) Quadratic (20-node) hexahedron[23]

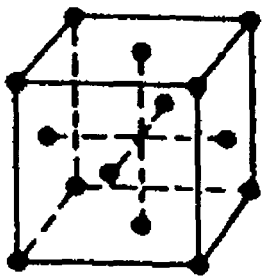

Figure 2.2 Unit cell of F.C.C. lattice[24]

If order $n=1$, the complete displacement field of one element using polynomials in three dimensions is:

$$u=\alpha_1+\alpha_2 x+\alpha_3 y+\alpha_4 z$$

$$v=\alpha_5+\alpha_6 x+\alpha_7 y+\alpha_8 z$$

$$w=\alpha_9+\alpha_{10} x+\alpha_{11} y+\alpha_{12} z \qquad (2.1)$$

The coefficients α_1 to α_{12} can be obtained by substituting four sets of node coordinates and displacements into equation (2.1), which results in generating the constant strain (four-node) tetrahedron element (figure 2.1(a)). The same idea is used to build displacement field when order $n=2$. The terms x^2, y^2, z^2, xy, yz, zx are added to equation (2.1), which is (ten-node) linear strain tetrahedron element (figure 2.2(b)). If $n=3$, ten more terms x^3, y^3, z^3, x^2y, xy^2, y^2z, yz^2, zx^2, z^2x and xyz added above $n=2$, which generates quadratic (20-node) hexahedron element (figure 2.1(d)) as well. Also, there is a special displacement field generation, which has eight terms and is the product of three linear polynomials $(\beta_1+\beta_2 x)(\beta_3+\beta_4 y)(\beta_5+\beta_6 z)$, which gives trilinear (eight-node) hexahedron (figure 2.1(c)) element. All above four-type elements satisfy the convergence requirement. However, from Figure 2.2, there are fourteen atoms in one unit cell of F.C.C. lattice. It is impractical to generate a displacement field using 14 nodes to meet convergence condition under the current method.

(ii) Interaction of atoms

Once the displacement field in one element is generated, the strain field in this element can be obtained by

$$\varepsilon_{ij} = \frac{\partial u_i}{\partial x_j} \tag{2.2}$$

Here strain ε_{ij}, displacement u_i and direction x_j are tensors and i and j are free indices in the three directions. The stress field of this element is evaluated from the strain field by a certain constitutive law. Then the internal force on every node can be obtained by equation (1.17). Therefore, the internal force of one node comes from the element(s) to which it is connected. However, under the action of potential energy of the system, the interaction of atoms could extend two or more unit cells. That is, the internal force of node i could come from other node j in the element on which atom i does not locate.

The above two factors in turn would create real problems in meshing such a material model under current Dynamic Relaxation techniques. The modification of Dynamic Relaxation algorithm is necessary.

2.2 Internal force

Fortunately, both pair potential energy functions and EAM potential functions are defined for separate atoms. They are polynomials or approximated by polynomials, so that the internal forces at the atoms can be easily obtained by the first derivative of potential energy functions.

2.2.1 Force from Lennard-Jones pair potential function

The equation (1.4) of Lennard-Jones pair potential function can be rewritten as

$$V(r_{ij}) = 4\left(\frac{1}{r_{ij}^{12}} - \frac{1}{r_{ij}^{6}}\right) = 4r_{ij}^{-12} - 4r_{ij}^{-6} \tag{2.3}$$

Suppose there is one pair of atoms i and j with coordinates (x_i, y_i, z_i) and (x_j, y_j, z_j) respectively. The distance between atom i and j is

$$r_{ij} = \sqrt{(x_i - x_j)^2 + (y_i - y_j)^2 + (z_i - z_j)^2} \tag{2.4}$$

The internal force in the x direction on the atom i is:

$$F_{ix} = -\frac{\partial V(r_{ij})}{\partial r_{ij}} \cdot \frac{\partial r_{ij}}{\partial x_i} = -(-48r_{ij}^{-13} + 24r_{ij}^{-7})\frac{2(x_i - x_j)}{2r_{ij}} = (48r_{ij}^{-14} - 24r_{ij}^{-8})(x_i - x_j) \tag{2.5}$$

The same approach is used for other coordinate directions:

$$F_{iy} = (48r_{ij}^{-14} - 24r_{ij}^{-8})(y_i - y_j) \tag{2.6}$$

$$F_{iz} = (48r_{ij}^{-14} - 24r_{ij}^{-8})(z_i - z_j) \tag{2.7}$$

For the atom j, the internal force components are:

$$\begin{Bmatrix} F_{jx} \\ F_{jy} \\ F_{jz} \end{Bmatrix} = -(48r_{ij}^{-14} - 24r_{ij}^{-8}) \begin{Bmatrix} (x_i - x_j) \\ (y_i - y_j) \\ (z_i - z_j) \end{Bmatrix} \tag{2.8}$$

Based on the above calculations, the total internal force on the atom i or j is obtained by summing all the interaction forces from atoms around it within the cut-off distance. For example, the net internal force components for atom i are:

$$\begin{Bmatrix} F_{ix}^{net} \\ F_{iy}^{net} \\ F_{iz}^{net} \end{Bmatrix} = -\sum_{j} \begin{Bmatrix} \dfrac{\partial V(r_{ij})}{\partial x_i} \\ \dfrac{\partial V(r_{ij})}{\partial y_i} \\ \dfrac{\partial V(r_{ij})}{\partial z_i} \end{Bmatrix} \tag{2.9}$$

2.2.2 Force from FS EAM potential function

Upon grouping equation (1.6) to (1.8), the potential energy of an atom i using FS EAM potential function is:

$$U_i(r_{ij}) = -\sqrt{\sum_{j} \phi(r_{ij})} + \frac{1}{2}\sum_{j} V(r_{ij}) \tag{2.10}$$

Here r_{ij} is the distance between atom i and j; $\phi(r_{ij})$ and $V(r_{ij})$ are defined in equation (1.10) and (1.11) respectively. Since the EAM potential energy function gives the total potential energy of one node, the net internal force on this node can be directly obtained by the first derivative of the EAM potential energy function. Still, the coordinates of atom i and any other atom j within the cut-off distance are (x_i, y_i, z_i) and (x_j, y_j, z_j). The

distance is calculated as equation (2.4).

The internal force components on atom i are:

$$F_{ix}^{net} = -\frac{dU_i(r_{ij})}{dr_{ij}} \cdot \frac{\partial r_{ij}}{\partial x_i}$$

$$= -\frac{1}{2}\left(\sum_j \phi(r_{ij})\right)^{-\frac{1}{2}} \cdot \sum_j \sum_{k=1}^{2} 3A_k (R_k - r_{ij})^2 \frac{(x_i - x_j)}{r_{ij}} H(R_k - r_{ij}) \qquad (2.11)$$

$$+\frac{1}{2}\sum_j \sum_{k=1}^{6} 3a_k (r_k - r_{ij})^2 \frac{(x_i - x_j)}{r_{ij}} H(r_k - r_{ij})$$

$$F_{iy}^{net} = -\frac{dU_i(r_{ij})}{dr_{ij}} \cdot \frac{\partial r_{ij}}{\partial y_i}$$

$$= -\frac{1}{2}\left(\sum_j \phi(r_{ij})\right)^{-\frac{1}{2}} \cdot \sum_j \sum_{k=1}^{2} 3A_k (R_k - r_{ij})^2 \frac{(y_i - y_j)}{r_{ij}} H(R_k - r_{ij}) \qquad (2.12)$$

$$+\frac{1}{2}\sum_j \sum_{k=1}^{6} 3a_k (r_k - r_{ij})^2 \frac{(y_i - y_j)}{r_{ij}} H(r_k - r_{ij})$$

$$F_{iz}^{net} = -\frac{dU_i(r_{ij})}{dr_{ij}} \cdot \frac{\partial r_{ij}}{\partial z_i}$$

$$= -\frac{1}{2}\left(\sum_j \phi(r_{ij})\right)^{-\frac{1}{2}} \cdot \sum_j \sum_{k=1}^{2} 3A_k (R_k - r_{ij})^2 \frac{(z_i - z_j)}{r_{ij}} H(R_k - r_{ij}) \qquad (2.13)$$

$$+\frac{1}{2}\sum_j \sum_{k=1}^{6} 3a_k (r_k - r_{ij})^2 \frac{(z_i - z_j)}{r_{ij}} H(r_k - r_{ij})$$

From equation (2.9) and equation (2.11) to (2.13), in the explicit Dynamic Relaxation techniques, the internal forces on the atoms in every time step are obtained by

the updated atom positions and not from the elements. Thus, the whole material model is meshless and only separate atoms (nodes) exist.

2.3 Stiffness and scaled mass

As stated in Chapter 1, the masses M of atoms are arbitrary while they need to maintain the stability of the system and enhance the rate of convergence, which are both related to the stiffness K of the system. Since the basic calculation unit is always one pair of atoms [equation (1.4), (1.10) and (1.11)] if using pair potential energy function or EAM potential energy function, the models can then be interpreted as a structure problems, i.e. spring-mass or truss. Thus, the maximum frequency of atom i could be estimated as:

$$\omega_{\max} = \sqrt{\frac{K_i}{M_i}} \tag{2.14}$$

Here K_i includes effects of all pairs of atoms within cut-off distance.

Generally, $\omega_{\max}$ is set to 2.0, then the critical time step is estimated as

$$\Delta t_{cr} = \frac{2}{\omega_{\max}} = 1.0 \tag{2.15}$$

so that computation is simplified. Since the whole material model is regarded as structure model, the method of adjusting the mass density in the continua to obtain scaled mass and critical time step is not suitable. The direct method is applied here. The mass of atom i can be scaled as[22]

$$M_i = \frac{1}{4} K_i \tag{2.16}$$

Like a spring-mass system, the stiffness of any atom can be obtained by second derivative of its potential energy. Based on this, three different ways to predict the stiffness K have been developed and tested:

2.3.1 Direct method

A straightforward method for calculating stiffness K comes from regular spring-mass model. In Figure 2.3, suppose that there are two atoms j and k around atom i within cut-off distance (one dimension). The stiffness of atom i is:

$$K_i = K_1 + K_2 \tag{2.17}$$

where K_1 is the stiffness between atoms i and j, and K_2 is the stiffness between atoms i and k. Higher dimensions or more atoms are addressed with same idea. For instance, from pair potential energy function in x direction,

$$K_{ix} = \sum_j \frac{\partial F_{ix}(x_i, x_j)}{\partial x_i} \tag{2.18}$$

From EAM potential energy function in x direction,

$$K_{ix} = \frac{\partial F_{ix}^{net}(x_i, x_j, \ldots.)}{\partial x_i} \tag{2.19}$$

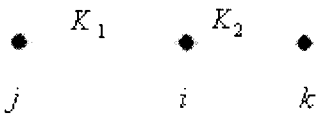

Figure 2.3 Three atoms model in one dimension

It is common to exhibit stiffness of the system clearly using matrix notation. In one dimension, the global stiffness of above system is:

$$\begin{array}{c} \\ i_x \\ j_x \\ k_x \end{array} \begin{array}{c} \begin{array}{ccc} i_x & j_x & k_x \end{array} \\ \begin{bmatrix} K_1 + K_2 & -K_1 & -K_2 \\ -K_1 & K_1 & 0 \\ -K_2 & 0 & K_2 \end{bmatrix} \end{array} \tag{2.20}$$

The mass matrix can be written as:

$$\begin{bmatrix} m_{ix} & 0 & 0 \\ 0 & m_{jx} & 0 \\ 0 & 0 & m_{kx} \end{bmatrix} = \frac{1}{4} \begin{bmatrix} K_1 + K_2 & 0 & 0 \\ 0 & K_1 & 0 \\ 0 & 0 & K_2 \end{bmatrix} \tag{2.21}$$

Thus, equation (2.16) is changed to

$$M_{ii} = \frac{1}{4} K_{ii} \tag{2.22}$$

where the subscript *ii* stands for the diagonal of the matrix.

After implementation, this method is not entirely successful because there are repulsive and attractive forces existing between atoms. When attractive force is dominant

at one atom, the stiffness shows a negative value, which is like a 'negative spring'. In figure 2.3, if attractive force is dominate between atom i and j while repulsive force is between atom i and k, K_1 and K_2 have opposite signs. If using equation (2.17) to estimate the stiffness, the estimated stiffness would be less than actual value so that the estimated participating natural frequency of the system [equation (1.36)] could be higher than the artificial maximum natural frequency [equation (2.14)]. Furthermore, if the net force on the atom is attractive force, the stiffness of the atom is negative and leads to negative mass value, which is not allowable since a system would be unstable.

2.3.2 Modified direct method

In order to avoid negative mass, an alternative, equation (2.22) is considered to change to

$$M_{ii} = \frac{1}{4}\left|K_{ii}\right| \tag{2.23}$$

To state it clearly, figure 2.3 is expanded to a 2D model as an example (figure 2.4). Still, two atoms j and k are around atom i within the cut-off distance (two dimension). Therefore, equation (2.18) and (2.19) can be changed to

$$K_{ix} = \sum_j \left|K_{ixix}^{ij}\right| = \sum_j \left|\frac{\partial F_{ix}(x_i, x_j)}{\partial x_i}\right| \tag{2.24}$$

$$K_{ix} = \sum_j \left|K_{ixix}^{ij}\right| = \left|\frac{\partial F_{ix}^{net}(x_i, x_j, \ldots.)}{\partial x_i}\right| \tag{2.25}$$

For higher dimensions, it is easy to change direction x_i to y_i and z_i to obtain stiffness in higher directions.

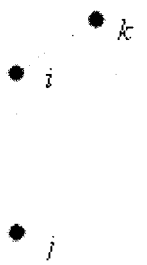

Figure 2.4 Three atoms model in two dimensions

The global stiffness matrix based on figure 2.4 is

$$
\begin{array}{c}
\\ i_x \\ i_y \\ j_x \\ j_y \\ k_x \\ k_y
\end{array}
\begin{array}{c}
\begin{array}{cccccc} i_x & i_y & j_x & j_y & k_x & k_y \end{array} \\
\begin{bmatrix}
\left|K^{ij}_{ixix}\right| + \left|K^{ik}_{ixix}\right| & \left|K^{ij}_{ixiy}\right| + \left|K^{ik}_{ixiy}\right| & K_{ixjx} & K_{ixjy} & K_{ixkx} & K_{ixky} \\
\left|K^{ij}_{iyix}\right| + \left|K^{ik}_{iyix}\right| & \left|K^{ij}_{iyiy}\right| + \left|K^{ik}_{iyiy}\right| & K_{iyjx} & K_{iyjy} & K_{iykx} & K_{iyky} \\
K_{jxix} & K_{jxiy} & \left|K^{ij}_{jxjx}\right| & K_{jxjy} & 0 & 0 \\
K_{jyix} & K_{jyiy} & K_{jyjx} & \left|K^{ij}_{jyjy}\right| & 0 & 0 \\
K_{kxix} & K_{kxiy} & 0 & 0 & \left|K^{ik}_{kxkx}\right| & K_{kxky} \\
K_{kyix} & K_{kyiy} & 0 & 0 & K_{kxky} & \left|K^{ik}_{kyky}\right|
\end{bmatrix}
\end{array}
\tag{2.26}
$$

and the mass matrix becomes the diagonal part of equation (2.26)

$$\begin{bmatrix} m_{ix} & 0 & 0 & 0 & 0 & 0 \\ 0 & m_{iy} & 0 & 0 & 0 & 0 \\ 0 & 0 & m_{jx} & 0 & 0 & 0 \\ 0 & 0 & 0 & m_{jy} & 0 & 0 \\ 0 & 0 & 0 & 0 & m_{kx} & 0 \\ 0 & 0 & 0 & 0 & 0 & m_{ky} \end{bmatrix} = \frac{1}{4} \begin{bmatrix} \left|K^{ij}_{ixix}\right| + \left|K^{ik}_{ixix}\right| & 0 & 0 & 0 & 0 & 0 \\ 0 & \left|K^{ij}_{iyiy}\right| + \left|K^{ik}_{iyiy}\right| & 0 & 0 & 0 & 0 \\ 0 & 0 & \left|K^{ij}_{jxjx}\right| & 0 & 0 & 0 \\ 0 & 0 & 0 & \left|K^{ij}_{jyjy}\right| & 0 & 0 \\ 0 & 0 & 0 & 0 & \left|K^{ik}_{kxkx}\right| & 0 \\ 0 & 0 & 0 & 0 & 0 & \left|K^{ik}_{kyky}\right| \end{bmatrix} \quad (2.27)$$

Thus, from equation (2.23) to (2.27), for a three-dimensional material model, the conclusion is that an atom has three mass values in three coordinate directions corresponding to absolute global stiffness values in three coordinate directions. Although, this estimation eliminates the negative mass, there are still a few difficulties to be addressed.

(a) Since stiffness is the second derivative of potential energy function, it needs to be decomposed into three components along the coordinate direction, which would consume much computer resources to calculate them.

(b) The absolute global diagonal stiffness value, as the summation of absolute value of local stiffness component(s), still has the risk to be less than actual stiffness value, which makes the natural frequency higher than the estimated maximum frequency of the system. Especially from EAM potential energy function, the stiffness of any atom is evaluated as an integrated value coming from all its neighboring atoms within cut-off distance [equation (2.25)] and cannot be calculated as summation of absolute components of local stiffness [e.g. item $i_1 i_1$ circled in equation (2.26)], which in turn makes it difficult to ensure that the participating natural frequency will be lower than estimated maximum frequency.

2.3.3 Method from Gerschgorin Circle Theorem

2.3.3.1 Analysis

The third method is based on Gerschgorin Circle Theorem[25], which states that:

Each (real or complex) eigenvalue λ of an $n \times n$ matrix $\boldsymbol{B}$ satisfies at least one of the inequalities:

$$|\lambda - b_{ii}| \le r_i, \quad r_i = \sum_{\substack{j=1 \\ j \neq i}}^{n} |b_{ij}| \tag{2.28}$$

where b_{ii} are the diagonal components of the matrix $\boldsymbol{B}$.

For the general mechanical system,

$$\mathbf{M}\ddot{\mathbf{x}} + \mathbf{K}\mathbf{x} = \mathbf{0} \tag{2.29}$$

then, equation (2.29) is changed to

$$\ddot{\mathbf{x}} + \mathbf{M}^{-1}\mathbf{K}\mathbf{x} = \mathbf{0} \tag{2.30}$$

Since mass matrix $\mathbf{M}$ is diagonal while stiffness matrix $\mathbf{K}$ is not, the matrix $\mathbf{M}^{-1}\mathbf{K}$ cannot be diagonal and it becomes difficult to decouple the system. The solution is to find eigenvalues of the matrix $\mathbf{M}^{-1}\mathbf{K}$. Based on equation (2.14), the eigenvalues of the matrix $\mathbf{M}^{-1}\mathbf{K}$ should be ω^2.

The eigenvalues of $\mathbf{M}^{-1}\mathbf{K}$ are defined by,

$$\mathbf{M}^{-1}\mathbf{K} - \lambda\mathbf{I} = \mathbf{0} \tag{2.31}$$

where λ is a series of eigenvalues and equals ω^2 . The global stiffness matrix can be structured as follows: Every pair of atoms within cut-off distance is regarded as an element. At this stage, a 1-D approach is used to find the stiffness for the element. For

example, in figure 2.4, atom i exists in two elements and atom j and k exist in one element respectively. For the purpose of scaling the mass, the global stiffness matrix ignores the orientation and becomes

$$\mathbf{K} = \begin{array}{c} \begin{matrix} i_x & i_y & \mathrm{j}_x & \mathrm{j}_y & k_x & k_y \end{matrix} \\ \begin{bmatrix} K_{ij}+K_{ik} & 0 & -K_{ij} & 0 & -K_{ik} & 0 \\ 0 & K_{ij}+K_{ik} & 0 & -K_{ij} & 0 & -K_{ik} \\ -K_{ij} & 0 & K_{ij} & 0 & 0 & 0 \\ 0 & -K_{ij} & 0 & K_{ij} & 0 & 0 \\ -K_{ik} & 0 & 0 & 0 & K_{ik} & 0 \\ 0 & -K_{ik} & 0 & 0 & 0 & K_{ik} \end{bmatrix} \end{array} \begin{matrix} i_x \\ i_y \\ j_x \\ j_y \\ k_x \\ k_y \end{matrix} \tag{2.32}$$

Implications of ignoring the orientation are discussed below.

In order to explain the approach, combine equations (2.28), (2.31) and (2.32) and use first row as an example to obtain

$$\left| \lambda - \frac{\left| K_{ij}+K_{ik} \right|}{m_{ix}} \right| \le \frac{\left| K_{ij} \right|}{m_{ix}} + \frac{\left| K_{ik} \right|}{m_{ix}} \tag{2.33}$$

Therefore,

$$\lambda \le \frac{\left| K_{ij} \right|}{m_{ix}} + \frac{\left| K_{ik} \right|}{m_{ix}} + \frac{\left| K_{ij}+K_{ik} \right|}{m_{ix}} \le 2\left(\frac{\left| K_{ij} \right|}{m_{ix}} + \frac{\left| K_{ik} \right|}{m_{ix}} \right) \tag{2.34}$$

Meanwhile,

$$\lambda \le \lambda_{\max} \le \frac{4}{\Delta t_{cr}^2} \quad \left(\text{because } \Delta t_{cr} \le \frac{2}{\omega_{\max}} \right) \tag{2.35}$$

Thus,

$$2\left(\frac{|K_{ij}|+|K_{ik}|}{m_{ix}}\right)\leq\frac{4}{\Delta t_{cr}^2} \tag{2.36}$$

Then

$$m_{ix}\geq\frac{1}{2}\left(|K_{ij}|+|K_{ik}|\right)\Delta t_{cr}^2=\frac{1}{2}\Delta t_{cr}^2\sum_{j\neq i}|K_{ij}| \tag{2.37}$$

From the above calculations, the mass value in three coordinate directions is same. Therefore, the general format of any atom, the mass still can be estimated as

$$m_i=\frac{1}{4}\sum_{j\neq i}|K_{ij}| \tag{2.38}$$

However, the critical time step Δt_{cr} should be scaled back to $\frac{\sqrt{2}}{2}$ to satisfy the inequality (2.37).

From the pair potential energy function [equation (2.3)],

$$m_i=\frac{1}{4}\sum_{j\neq i}\left|-\frac{d^2V(r_{ij})}{dr_{ij}^2}\right|=\sum_{j\neq i}\left|-624r_{ij}^{-14}+168r_{ij}^{-8}\right| \tag{2.39}$$

From EAM potential energy function [equation (1.10), (1.11) and (2.10)],

$$m_i=\frac{1}{4}\left|-\frac{d^2U_i(r_{ij})}{dr_{ij}^2}\right|$$

$$=\frac{1}{4}\left|\underbrace{-\frac{1}{4}\left(\sum_j\phi(r_{ij})\right)^{-\frac{3}{2}}\left(\sum_j\frac{d\phi(r_{ij})}{dr_{ij}}\right)^2}_{(1)}+\underbrace{\frac{1}{2}\left(\sum_j\phi(r_{ij})\right)^{-\frac{1}{2}}\sum_j\frac{d^2\phi(r_{ij})}{dr_{ij}^2}}_{(2)}-\underbrace{\frac{1}{2}\sum_j\frac{d^2V(r_{ij})}{dr_{ij}^2}}_{(3)}\right| \tag{2.40}$$

where

$$\frac{d\phi(r_{ij})}{dr_{ij}} = \sum_{k=1}^{2}(-3)\times A_k \times (R_k - r_{ij})^2 \times H(R_k - r_{ij}) \tag{2.41}$$

$$\frac{d^2\phi(r_{ij})}{dr_{ij}^2} = \sum_{k=1}^{2} 6\times A_k \times (R_k - r_{ij}) \times H(R_k - r_{ij}) \tag{2.42}$$

$$\frac{d^2V(r_{ij})}{dr_{ij}^2} = \sum_{k=1}^{6} 6\times a_k \times (r_k - r_{ij}) \times H(r_k - r_{ij}) \tag{2.43}$$

As mentioned in chapter 2.3.2(b), it is a challenge for EAM potential energy function to generate stiffness to adapt equation (2.38). After testing several cases, it was found that:

(i) The summation of item (1) and item (2) in equation (2.40) is less than 5% of the value of item (3)

(ii) The summation of item (1) and item (2) has the opposite sign of item (3).

Therefore the approximation is made: item (1) and (2) are omitted in the calculation of stiffness from EAM potential energy function. This procedure effectively enlarges the stiffness a little bit, but it is safe and conservative for the simulation. Thus, equation (2.40) is approximated to

$$m_i = \frac{1}{4}\sum_{j\neq i}\left|-\frac{1}{2}\frac{d^2V(r_{ij})}{dr_{ij}^2}\right| = \frac{1}{4}\sum_{j\neq i}\left|-\frac{1}{2}\sum_{k=1}^{6} 6\times a_k \times (r_k - r_{ij}) \times H(r_k - r_{ij})\right| \tag{2.44}$$

2.3.3.2 Discussion of mass scaling

Utilizing method (3) to estimate stiffness can simplify the calculation compared to the method (2). Meanwhile, method (3) ensures that the participating natural frequency is lower than maximum frequency of the system. However, the stiffness from Gerschgorim estimation [equation (2.37)] may be greater than actual stiffness values. Then the participating frequency of the overall model could be much lower than the highest frequency so that the convergence rate is reduced.

The above mass estimation is based on equation (2.38) and is revised every time step. Due to the highly non-linear nature of the potential energy functions, the stiffness, along with the mass, changes much faster than general structural problems. This may adversely affect the progress of solutions. An alternative approach is to fix the mass during the entire simulation. The mass value is obtained by method (3) above in the first time step and then this value is kept constant through the simulation. The stiffness is still updated by method (3) in every time step. Here,

$$\omega_{\max} = Max\left(\sqrt{\frac{K_i}{m_i}}\right), \quad i = 1, \cdots, n \tag{2.45}$$

Then, the critical time step is changed by every time step.

$$\Delta t_{cr} = \delta \frac{2}{\omega_{\max}} \tag{2.46}$$

The coefficient δ is used to scale back the critical time step according to inequality (2.37). According to the numerical tests carried out so far, $\delta = 0.5 \sim 0.7$ is safe to stabilize

the simulation.

2.3 Damping

In order to control the manner in which the system approaches equilibrium, mass proportional critical damping is used during the simulation. Referred to equation (1.25), damping formula is changed to:

$$C = 2\xi\omega M \tag{2.47}$$

Here ω is defined in equation (1.34) and ξ is damping ratio. In the regular Dynamic Relaxation algorithm for finite element analysis, ξ value is usually set to 1.0 in order to apply critical damping into system to get maximum convergence rate. Setting ξ above or below 1.0 reduces the convergence speed.

In the atomistic model, the damping ratio is more than an indicator of the convergence rate. Because damping dissipates the kinetic energy of the system, the results of relaxation are always obtained at the temperature of absolute zero (0K) when no kinetic energy exists. When applying a damping ratio, the system can experience higher kinetic energy (higher temperature) prior to reaching the equilibrium so atoms have more opportunity to move into new configurations. This in turn may require more time steps to get convergence. Contrarily, applying a high damping ratio affects maximum kinetic energy of the system so that the atoms are less likely to move into new configurations and could stop at local equilibrium positions. This may converge in a shorter time.

The conclusion is that the damping ratio affects the solution path so that a different damping ratio could lead to different minimum potential energy and equilibrium shapes. More details of the numerical responses after applying different damping ratio will be considered in detail in Chapter 3.

2.4 Convergence criterion

Dynamic Relaxation is based on viewing the solution of a static problem as the steady-state solution, equation (1.29), of a damped dynamic problem. Since the external forces have not been applied to the system yet, all the structure changes are the result from the internal forces. Therefore, the steady-state solution for the system means that:

$$\mathbf{F}_{\text{int}}^{t} = \mathbf{F}_{ext}^{t} = 0 \tag{2.48}$$

which is achieved when the simulation is finished.

When atoms find equilibrium positions, the potential energy could be either at a local minimum or at the global minimum and could converge to a constant value. According to equation (2.48), at this time, the first derivative of the potential energy functions or the summation of internal force vectors equals zero. Meanwhile, the rate of displacement (velocity) should be zero too. Referred to equation (1.37) and (1.38), the following two inequalities are the convergence criteria:

$$\left\| \mathbf{F}_{\text{int}}^{t} \right\|_2 < f_{tol} \tag{2.49}$$

$$\frac{\left\| \Delta t \dot{\mathbf{x}}^{t+\Delta t/2} \right\|_2}{\left\| \mathbf{u}^{t+\Delta t} \right\|_2} < u_{tol} \tag{2.50}$$

where $\| \ \|_2$ denotes Euclidean norm and f_{tol}, u_{tol} are tolerance values, which are set before the simulation. Meanwhile, inequality (2.49) could be changed to the dimensionless format.

$$\frac{\left\| \mathbf{F}_{\text{int}}^{t} \right\|_2}{Max(\left\| \mathbf{F}_{\text{int}} \right\|_2)} < f_{tol} \tag{2.51}$$

After examining above three convergence criteria, equation (2.50) is found not to be practicable. Due to the properties of the atomistic model, the re-arrangement of atoms in the defect area during the relaxation is small. Therefore, the change of displacement is much smaller than the change of interaction forces. In the simulation, when the internal force is still large, the rate of displacement could be very tiny already. In order to balance the efficiency for the simulation and accuracy for the result, inequality (2.50) is omitted.

Generally, when applying damping to the system, the internal force in the first step is largest. However, when applying lower damping to the system, the maximum internal force may be changing. Therefore inequality (2.51) could be used as convergence criteria to the system whose maximum internal force does not change.

Since the convergence rate is dependent on the number of atoms in the system, inequality (2.49) is used for small block of atoms with lower damping ratio and f_{tol} is set to 0.1 while inequality (2.51) is used for general cases and f_{tol} is changed to 0.01.

In some cases, the simulation cannot be stopped since oscillatory response sets in above the tolerance value. One possible reason is the EAM potential energy functions

could exhibit oscillatory response due to the bulk effect[5] if there free surfaces exist. In order to stop the computation, a maximum number of cycles is set in the algorithm. If the cycle number is beyond the maximum, the program is terminated automatically and the progress toward convergence must be examined.

2.5 Boundary Conditions

A small piece of metal consists of billions of atoms. Practically, it is common to simulate thousands of atoms for the specific problem. In order to mimic the real systems, applying boundary condition is an essential task.

In this thesis, three kinds of boundary conditions are used and examined:

(1) Free boundary condition

Under the free boundary condition, all degrees of freedom or certain coordinate directions are free for the atoms (nodes). In the cases discussed in Chapter 3, free surfaces are used. Although the material model with free boundary condition may not be used to mimic reality, many numerical responses are revealed and can be studied.

(2) Fixed boundary condition

Under the fixed boundary condition, all degrees of freedom or certain coordinate directions are fixed for the atoms (nodes). The fixed boundary condition is widely used as a physical boundary of the model.

(3) Periodic boundary condition

In order to simulate bulk phases, employing periodic boundary condition is a key method to mimic the presence of an infinite bulk material surrounding a N-atom material model system. The model containing the N atoms is treated as the primitive cell of an infinite periodic lattice of identical cells. In figure 2.5, any atom i interacts with all other atoms within a cut-off distance in the infinite periodic system. All other atoms include the atoms in the primitive cell and in all its image cells.[1]

2.5.1 Periodic boundaries

In the atomistic simulation, when applying periodic boundary condition to the model, the internal forces should be identical on certain atom and on all corresponding images. Therefore, the atom and its all images should have the same acceleration, which means the atom and its all images have uniform motion.

The key points for calculating periodic boundary condition are as follows:

(1) For 3-D material model, applying periodic boundary condition to one coordinate direction is widely used. Sometimes, it is also applied to two coordinate directions of the model. However, it is rare to apply it to all three coordinate directions. This thesis studies the periodic boundary condition in one dimension and two dimensions. For a given atom i, there are two images in one dimension (figure 2.6) and 8 images in two dimensions (figure 2.7).

(2) Generally, the cut-off distance r_c must be less than half the length of the primitive

cell r_L in any coordinate direction. Otherwise, some image atoms could be missed or double counted.

(3) The distance r_{ij} between any atom i and j now is determined by atom $i(x_i, y_i, z_i)$, atom $j(x_j, y_j, z_j)$ and all atom j's images if fixing the position of atom i. For 1-D x direction periodic symmetry, first evaluate the distance r_{ij}. If $r_{ij} > r_c$, then evaluate the distance between atom i and two images of atom j: $j_1\ (x_j + r_L, y_j, z_j)$ and $j_2\ (x_j - r_L, y_j, z_j)$. Three circumstances are listed as follows:

(a) If neither r_{ij1} nor r_{ij2} is in the cut-off distance r_c, atom j is skipped;

(b) If either r_{ij1} or r_{ij2} is within the cut-off distance, this value is the distance between atom i and j;

(c) if both r_{ij1} and r_{ij2} are within the cut-off distance r_c, choose minimum value in r_{ij1} and r_{ij2} to determine the distance r_{ij}.

(4) For 2-D periodic symmetry in the x, y directions, the calculation procedure is the same as for 1-D problem, which was discussed in (3). The only difference is that there are eight images of atom j. They are:

$j_1(x_j + r_L, y_i, z_i)$, $j_2(x_j - r_L, y_j, z_j)$, $j_3(x_j, y_j + r_L, z_j)$, $j_4(x_j, y_j - r_L, z_j)$, $j_5(x_j - r_L, y_j - r_L, z_j)$, $j_6(x_j + r_L, y_i - r_L, z_i)$, $j_7(x_j - r_L, y_j + r_L, z_j)$ and $j_8(x_j + r_L, y_i + r_L, z_i)$.

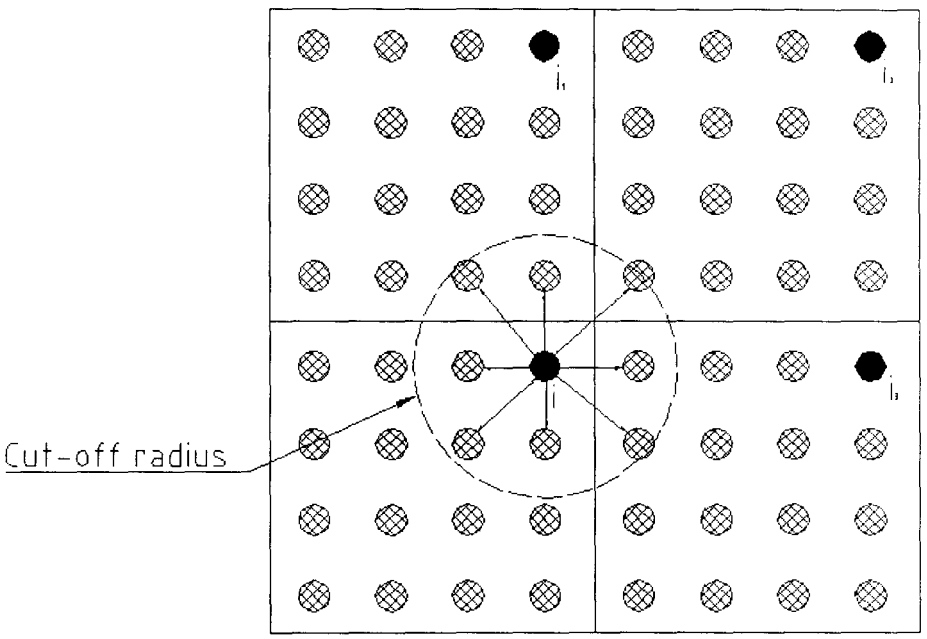

Figure 2.5 Scheme of periodic boundary condition

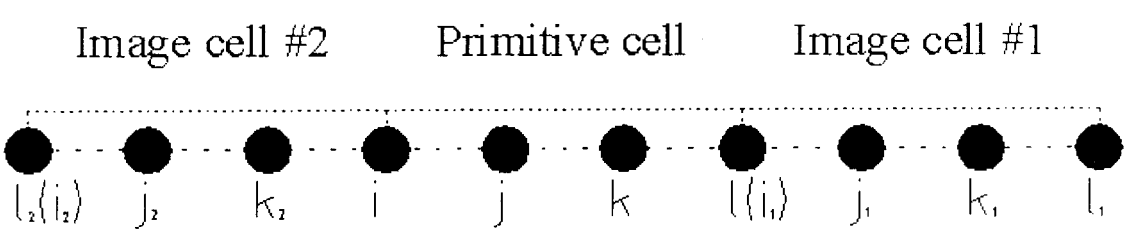

Figure 2.6 Periodic symmetry in one dimension

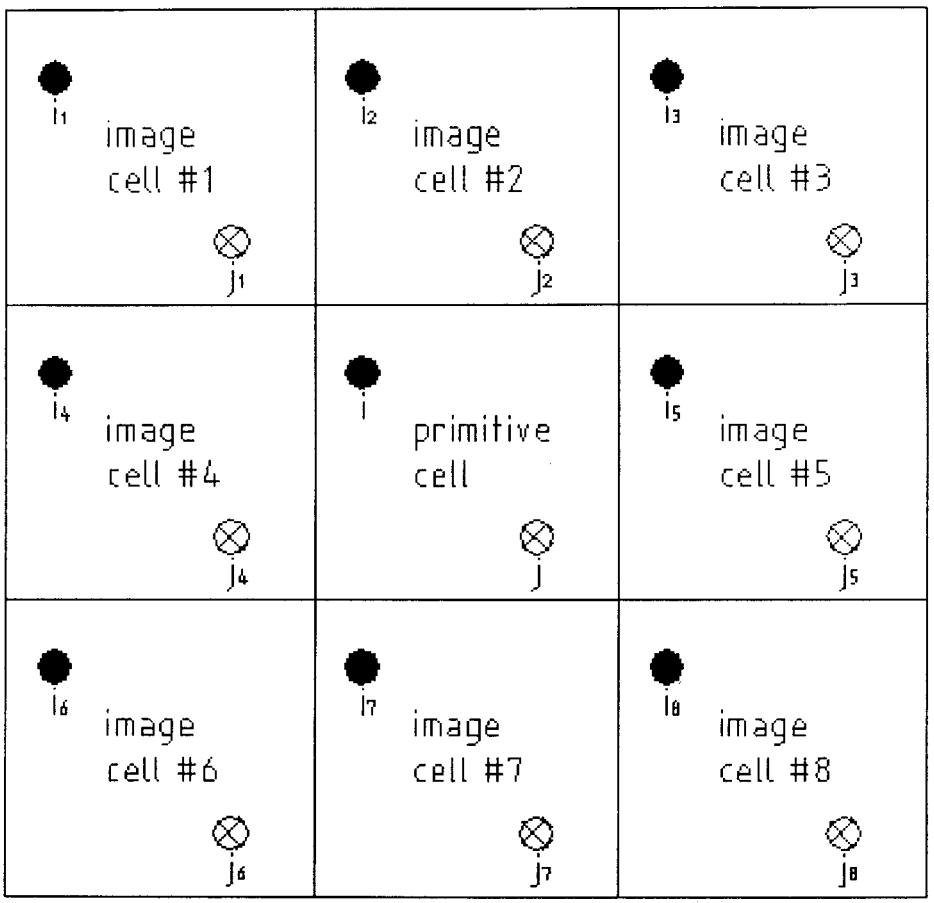

Figure 2.7 Periodic symmetry in two dimensions

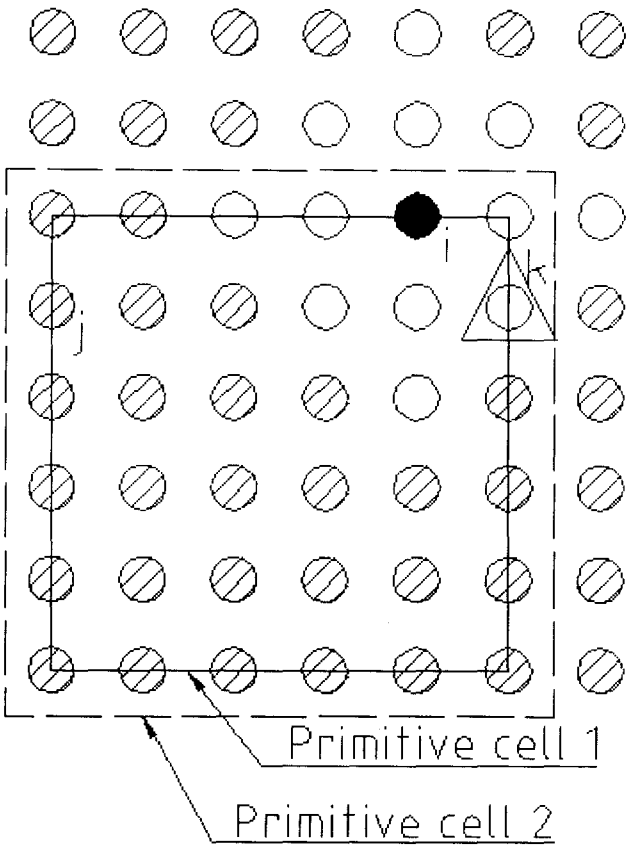

Figure 2.8 Scheme of coincident atoms

(5) For 2-D or 3-D models using periodic symmetry, there is a problem with coincident atoms. For example, in figure 2.8, there are 6×6 atoms in the model (primitive cell) and the cut-off distance r_c is to cover two nearest neighbors. Figure 2.8 shows how to calculate the properties of the atom *i* (black circle) in a given certain time step. The white circles indicate atoms located in the primitive cell and image cells, which interact with atom *i* within r_c. After calculating the distance r_{ij} between atom *i* and *j*, it is found that $r_{ij} > r_c$. Then all the atom *j*'s

images are searched. Atom *k*, as one of the images of atom *j*, has minimum distance with atom *i*. Thus, atom *k* is counted. Meanwhile, atom *k* itself is within the cut-off distance with atom *i*, so it is counted again. Therefore, the position of atom *k* is calculated twice, which is not correct in the simulation. The solution for the coincident atoms problem in this thesis is to build a neighbor list for any atom while calculating the distance with its neighbor atoms. If the position of one neighbor atom is on the list, that means that this position was calculated before and this atom is skipped. Second alternative solution is to increase one more unit cell length (half in the each side) to the original primitive cell (primitive cell 1, solid line in figure 2.8), which makes new primitive cell (primitive cell 2, dash line in figure 2.8). While the first solution is straightforward, the second one is perhaps more easily implemented.

2.6 Summary

Above features are major changes of Dynamic Relaxation algorithm. Table 2.1 and 2.2 summarize the modified algorithms, which represent changing mass and fixed mass algorithms respectively.

Table 2.1 Meshless Dynamic Relaxation Algorithm (changing mass)

I. Get F_{int} from initial position and initialize M for $\Delta t_{cr} = 0.707$ for each atom (node), set $\Delta t = 0.5 \sim 0.7$. Set damping ratio ξ.

II. At cycle n, time t

(i) $\ddot{x}^t = M^{-1} F_{\text{int}}^t$

(ii) $\dot{x}^{t+\Delta t/2} = \dfrac{(1-\xi\omega\Delta t)}{(1+\xi\omega\Delta t)} \dot{x}^{t-\Delta t/2} + \dfrac{\Delta t}{(1+\xi\omega\Delta t)} \ddot{x}^t$

$u^{t+\Delta t} = u^t + \Delta t \dot{x}^{t+\Delta t/2}$

$x^{t+\Delta t} = x^t + \Delta t \dot{x}^{t+\Delta t/2}$

(iii) Check error norm

$$\frac{\left\| \mathbf{F}_{\text{int}}^t \right\|_2}{Max\left(\left\| \mathbf{F}_{\text{int}} \right\|_2 \right)} < f_{tol} \quad \text{or} \quad \left\| \mathbf{F}_{\text{int}}^t \right\|_2 < f_{tol}$$

If not satisfied, cycle $n+1$, time $t+\Delta t$.

Check $n+1 < 250000$

If not satisfied, go to (iv)

Else, the program is terminated.

(iv) Obtain current internal force vector

$F_{\text{int}}^{t+\Delta t}$ and adjust M to set $\Delta t_{cr} = 0.707$

and let $\Delta t = 0.5 \sim 0.7$.

(v) Obtain current estimate of ω

$K_{ii}^t = \dot{x}^{t+\Delta t/2} (F_{\text{int}}^{t+\Delta t} - F_{\text{int}}^t) / \Delta t$

$K_{ii}^t = \max(K_{ii}^t, 0)$

$$\omega = \left[\frac{\sum K_{ii}^t}{\sum M_{ii} (\dot{x}^{t+\Delta t/2})^2} \right]^{1/2}$$

(vi) Go to (i) and repeat

Table 2.2 Meshless Dynamic Relaxation Algorithm (fixed mass)

I. Get F_{int} from initial position and initialize M for $\Delta t_{cr} = 0.707$ for each atom (node), set $\Delta t = 0.5 \sim 0.7$. Set damping ratio ξ.

II. At cycle n, time t

(i) $\ddot{x}^t = M^{-1} F_{\text{int}}^t$

(ii) $\dot{x}^{t+\Delta t/2} = \dfrac{(1-\xi\omega\Delta t)}{(1+\xi\omega\Delta t)} \dot{x}^{t-\Delta t/2} + \dfrac{\Delta t}{(1+\xi\omega\Delta t)} \ddot{x}^t$

$u^{t+\Delta t} = u^t + \Delta t \dot{x}^{t+\Delta t/2}$

$x^{t+\Delta t} = x^t + \Delta t \dot{x}^{t+\Delta t/2}$

(iii) Check error norm

$$\frac{\left\| \mathbf{F}_{\text{int}}^t \right\|_2}{Max\left(\left\| \mathbf{F}_{\text{int}} \right\|_2 \right)} < f_{tol} \quad \text{or} \quad \left\| \mathbf{F}_{\text{int}}^t \right\|_2 < f_{tol}$$

If not satisfied, cycle $n+1$, time $t+\Delta t$.

Check $n+1 < 250000$

If not satisfied, go to (iv)

Else, the program is terminated.

(iv) Obtain current internal force vector

$F_{\text{int}}^{t+\Delta t}$ and $\omega_{\max}$. $\Delta t_{cr} = \dfrac{2}{\omega_{\max}}$

and let $\Delta t_{n+1} = 0.5 \sim 0.7 \Delta t_{cr}$.

(v) Obtain current estimate of ω

$K_{ii}^t = \dot{x}^{t+\Delta t/2} (F_{\text{int}}^{t+\Delta t} - F_{\text{int}}^t) / \Delta t_{n+1}$

$K_{ii}^t = \max(K_{ii}^t, 0)$

$$\omega = \left[\frac{\sum K_{ii}^t}{\sum M_{ii} (\dot{x}^{t+\Delta t/2})^2} \right]^{1/2}$$

(vi) Go to (i) and repeat

CHAPTER 3 – NUMERICAL RESPONSE OF MODIFIED DYNAMIC RELAXATION ALGORITHM

In order to demonstrate numerical responses and results using modified Dynamic Relaxation techniques, four cases are presented. They describe problems including 1D, 2D and 3D, free surfaces, free body and periodic boundary conditions, different damping ratios, pair potential and EAM potential. Furthermore, certain difficulties which arise during the simulation are discussed. The purpose of this chapter is to implement and test the meshless Dynamic Relaxation algorithm and therefore some of these models may not have practical meaning for real materials. All the cases are based on a small block of atoms. In the practical simulation in order to study the properties of materials, the number of atoms should be appreciably larger. The practical model is presented in Chapter 4.

3.1 One-dimensional two-atom model

3.1.1 Model description

The series of tests start from the simplest model. The model contains two atoms, one of which is fixed (figure 3.1). Another atom is restricted to move in one dimension (x direction) and will be placed in the repulsion and attraction area. The Lennard-Jones pair

potential energy function is applied here.

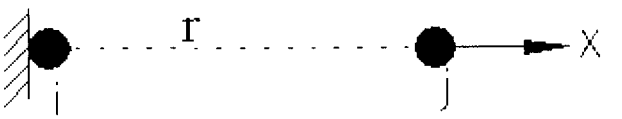

Figure 3.1 One dimension two-atom model

3.1.2 Analysis

Since the position of atom *i* is fixed, the change of potential energy of the above system is dependent on the position of atom *j*. The potential energy of the system is minimum when atom *j* arrives at its equilibrium position. The coordinate of atom *i* is set to zero. The equilibrium distance r_{ij} between atom *i* and *j* can be obtained by

$$\frac{dV(r_{ij})}{dr_{ij}} = 0 \tag{3.1}$$

According to equation (2.3),

$$-48r_{ij}^{-13} + 24r_{ij}^{-7} = 0 \tag{3.2}$$

Solved by *Matlab*[26], $r_{ij} \approx 1.12$ arbitrary units. The atom *j* is in the repulsion area when r_{ij} is less than 1.12 arbitrary units while atom *j* is in the attraction area when r_{ij} is larger than 1.12 arbitrary units.

3.1.3 Test results

(a) Position, potential energy and internal force

The coordinate of atom *j* is initially placed at 0.7 and 1.5 arbitrary units for the tests, which are approximately equal distance to the equilibrium point. Figure 3.2 to 3.4 show their time histories of the position of atom *j* (figure 3.2), time histories of the potential energy (figure 3.3) and the time history of the internal force (figure 3.4). For potential energy and internal force, the LOG10 and ABS function are used to draw the graphs, e.g. LOG10(ABS(potential energy)).

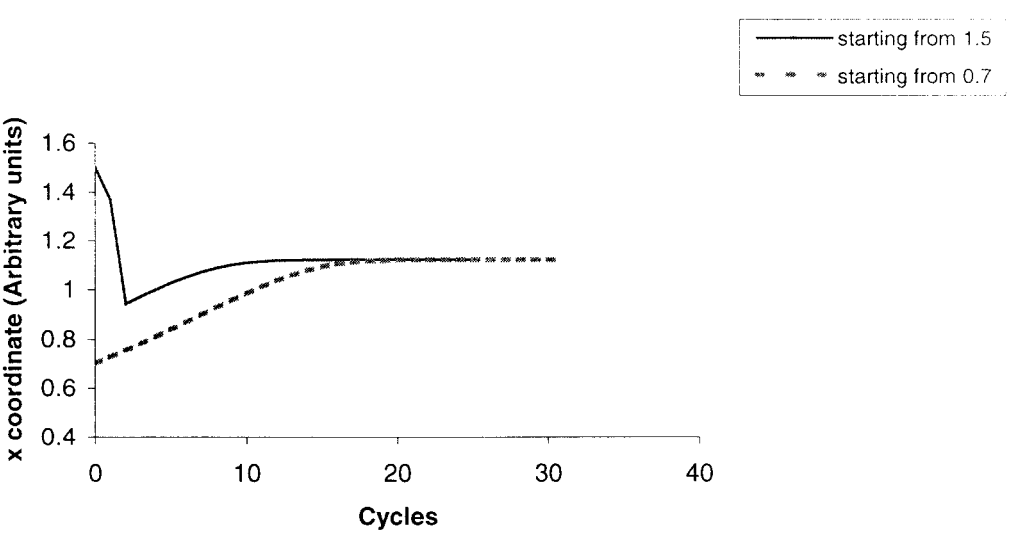

Figure 3.2 Position of atom *j* as a function of simulation time for 1D model (damping ratio 1.0)

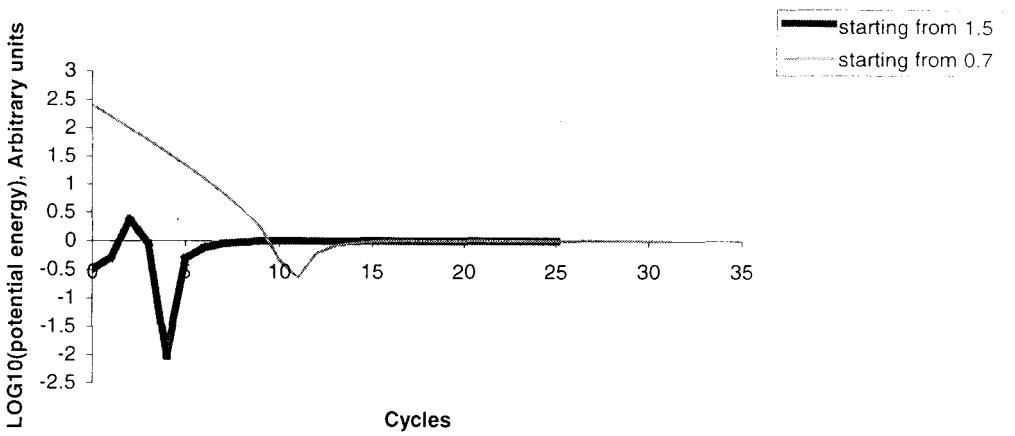

Figure 3.3 Potential energy of atom *j* as a function of simulation time for 1D model

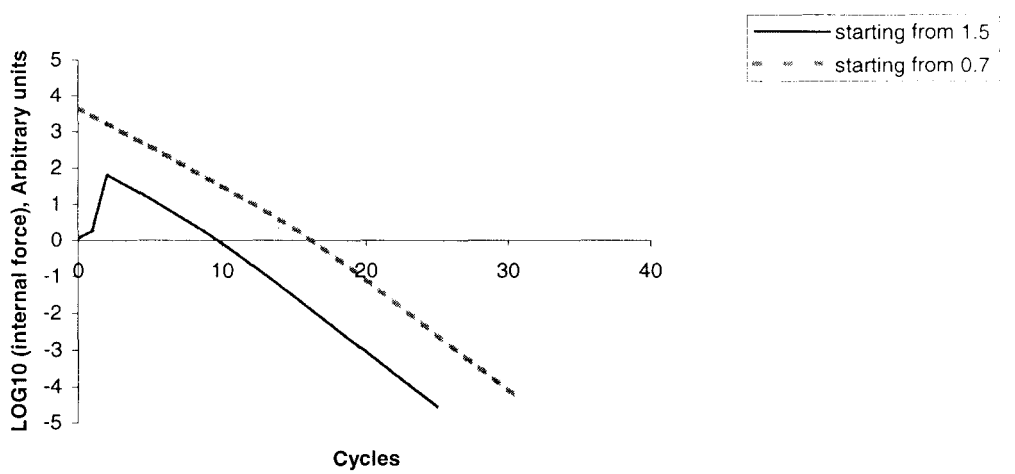

Figure 3.4 Internal force of atom *j* as a function of simulation time for 1D model

(b) Two algorithms

The changing mass (table 2.1) and fixed mass (table 2.2) algorithms are tested here. Atom *j* is initially placed in 1.5 arbitrary units. Figure 3.5 compares the time histories of positions of atom *j* while figure 3.6 compares the time histories of internal force for the two algorithms.

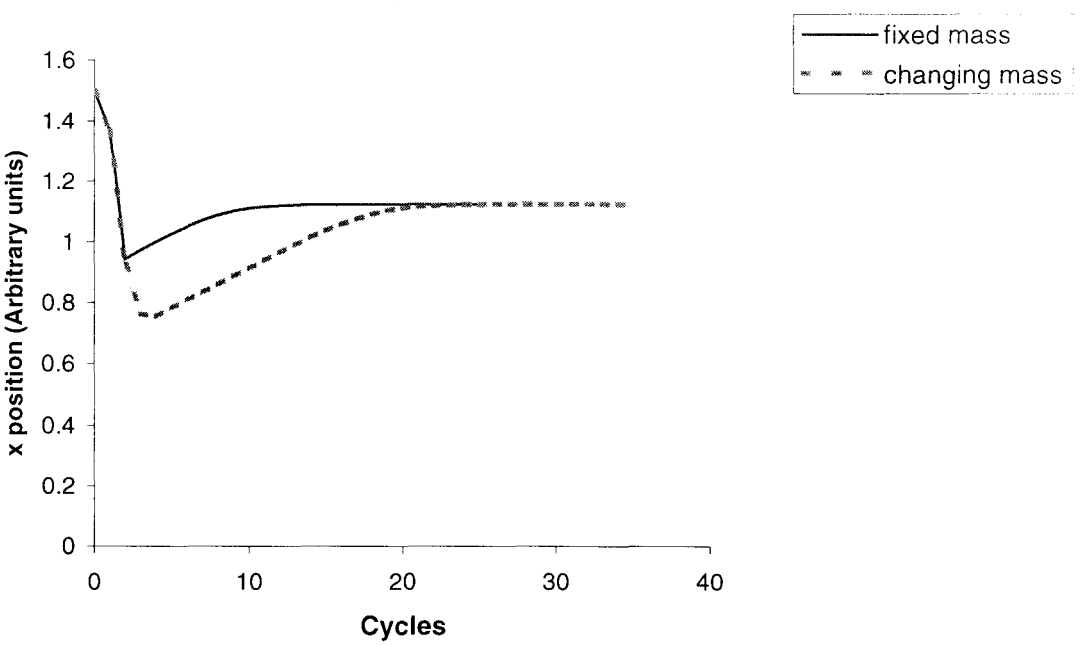

Figure 3.5 Positions of atom *j* as a function of simulation time for 1D model (damping ratio 1.0 and starting position was at 1.5 arbitrary units)

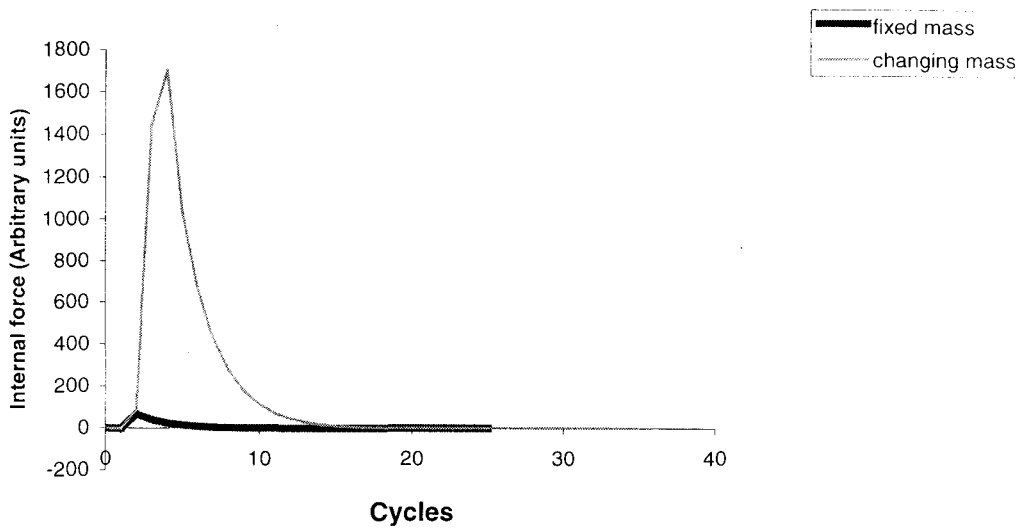

Figure 3.6 Internal force of atom *j* as a function of simulation time for 1D model (starting position was at 1.5 arbitrary units)

3.1.4 Discussion of results in one-dimensional model

(1) From figure 3.2, atom *j* initially in the attraction and repulsion area both converges to the equilibrium point at the end, which is in line with the analysis in 3.1.2. Meanwhile, atom *j* stops at the right place and shows that the modified Dynamic Relaxation algorithm works.

(2) From figures 3.3 and 3.4, the potential energy, along with the internal force, increases and changes rapidly when atom *j* enters the repulsion area. Therefore, for the same distance to the equilibrium point, atom *j* initially in the repulsion area has more energy

and is more active than when the atom j is initially in the attraction area, which leads to difficultly converging to the equilibrium point for atom j starting from the repulsion area.

(3) Since the attractive force is weak compared to the repulsive force under pair potential energy function, and the attractive force is becoming weaker and weaker when the atom moves farther and farther away from the equilibrium point, care must be taken when applying the external force when attractive force dominates in the system. If the amount of external force is not appropriate, the system may respond as if exploding.

(4) From figures 3.5 and 3.6, the amplitude of oscillation of position and internal force of atom j during convergence using changing mass algorithm is higher than using the fixed mass algorithm because mass is changed too fast compared to regular structural problems due to the highly non-linear pair potential energy function. Based on this, using the fixed mass algorithm could reduce convergence time.

3.2 Two-dimensional lattice

3.2.1 Model description

A two-dimensional lattice model is used to study the minimum potential energy configuration and learn the difference in results of a model with no boundary constraints (free body) and applying periodic boundary condition.

As shown in figure 3.7, the model consists of 6×6 atoms arranged in the primitive lattice, so that the distance between two columns and rows are equal. The spacing between atoms is 0.8 arbitrary units and the cut-off radius is set to cover two nearest neighbors. The potential energy is calculated by Lennard-Jones pair potential functions. The damping ratio is set to 2.0 to avoid possibly large oscillation.

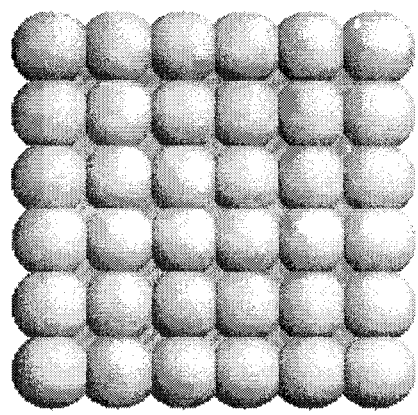

Figure 3.7 Initial configuration of two-dimensional lattice model

3.2.2 Analysis

To simplify the theoretical calculation, suppose that there are four atoms arranged as in figure 3.8. The total potential energy of the system is based on angle ϕ and equilibrium spacing r.

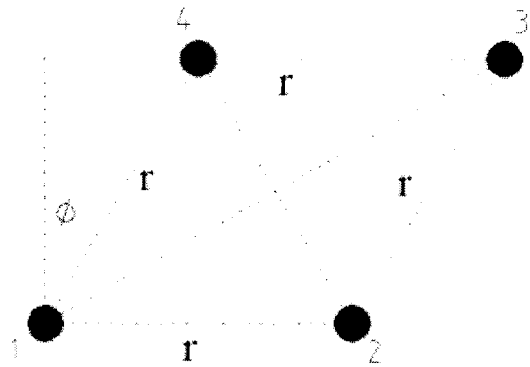

Figure 3.8 Parallelogram of four atoms

The angle ϕ and equilibrium spacing r between the atoms can be obtained at the minimum value of the global potential energy, for which:

$$\frac{\partial u_{total}(r,\phi)}{\partial \phi} = 0 \tag{3.3}$$

$$\frac{\partial u_{total}(r,\phi)}{\partial r} = 0 \tag{3.4}$$

Based on the Cosine Rule used for the system in figure 3.8,

$$r_{13} = \sqrt{r^2 + r^2 - 2r^2\cos(90^\circ + \phi)} = \sqrt{2r^2 + 2r^2\sin\phi} \tag{3.5}$$

$$r_{24} = \sqrt{r^2 + r^2 - 2r^2\cos(90^\circ - \phi)} = \sqrt{2r^2 - 2r^2\sin\phi} \tag{3.6}$$

Thus,

$$\begin{aligned} u_{total} &= V(r_{12}) + V(r_{23}) + V(r_{34}) + V(r_{14}) + V(r_{24}) + V(r_{13}) \\ &= 16r^{-12} - 16r^{-6} + 4(2r^2 - 2r^2\sin\phi)^{-6} - 4(2r^2 - 2r^2\sin\phi)^{-3} \\ &\quad + 4(2r^2 + 2r^2\sin\phi)^{-6} - 4(2r^2 + 2r^2\sin\phi)^{-3} \end{aligned} \tag{3.7}$$

According to equation (3.3) and (3.4), there are two equations with two unknowns:

$$2\times(2r^2)^{-3}\times[(1-\sin\phi)^{-7} - (1+\sin\phi)^{-7}] - (1-\sin\phi)^{-4} + (1+\sin\phi)^{-4} = 0 \tag{3.8}$$

$$\begin{aligned} &-192r^{-13} + 96r^{-7} - 24(2r^2 - 2r^2\sin\phi)^{-7}(4r - 4r\sin\phi) \\ &+12(2r^2 - 2r^2\sin\phi)^{-4}(4r - 4r\sin\phi) - 24(2r^2 + 2r^2\sin\phi)^{-7}(4r + 4r\sin\phi) \\ &+12(2r^2 + 2r^2\sin\phi)^{-4}(4r + 4r\sin\phi) = 0 \end{aligned} \tag{3.9}$$

Using numerical method to solve above equations by *Maple*[27], r is 1.120 and ϕ is 29.729° respectively.

3.2.3 Test results and discussion

(a) Cubic configuration with no restraints

Simulated relaxation result is obtained for the model shown in figure 3.7. Figure 3.9 shows the configuration after the relaxation and figure 3.10 is the time history of the potential energy.

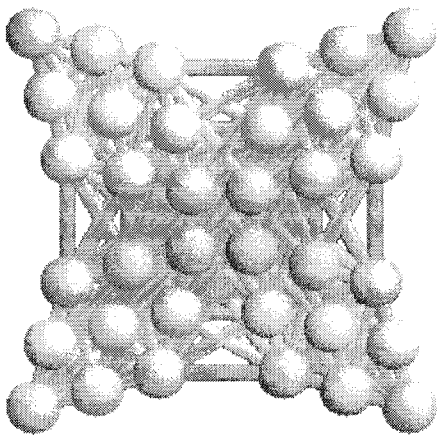

Figure 3.9 Configuration after the relaxation

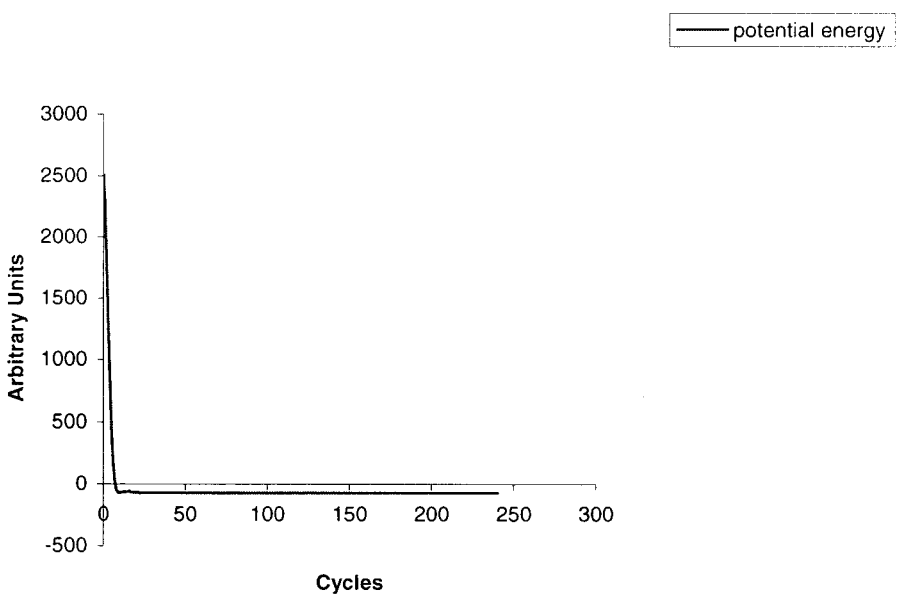

Figure 3.10 Potential energy as a function of simulation time for 2D model with free boundary condition

From figure 3.9, there are four symmetric regions of close-packed atoms, which are separated by gaps. This is because the internal force caused the atoms at the corner to move more readily than other atoms. In every region, the shape matches the analysis in 3.2.2.

As observed in figure 3.10, the potential energy goes down very quickly and converges to –74 arbitrary units.

(b) Close-packed configuration with no constraints

Compared to the test (a), this test examines if the close-packed atoms with no gap will have lower potential energy. The configuration of atoms following the analysis of 3.2.2 is constructed (figure 3.11). The spacing and angle of above model are chosen as 1.11 arbitrary units and 30°.

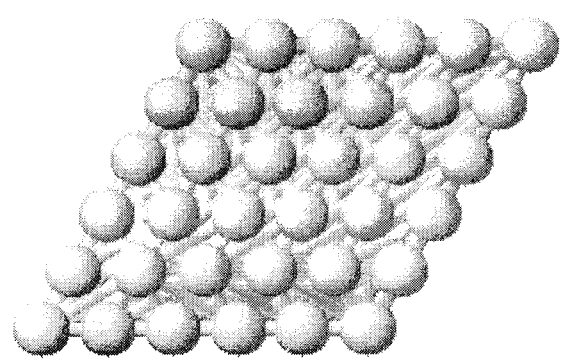

Figure 3.11 Configuration of atoms for test (b)

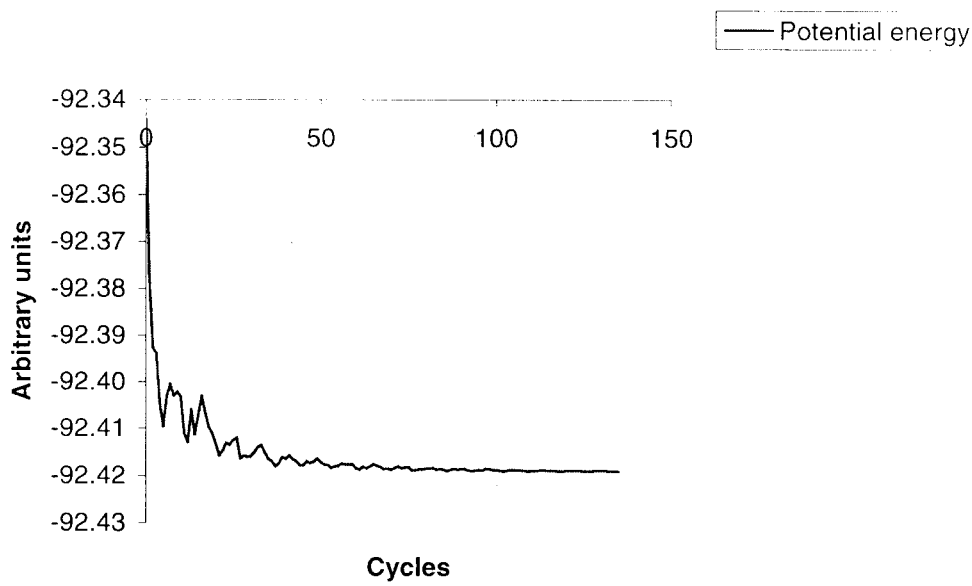

Figure 3.12 Potential energy as a function of simulation time for 2D model with no boundary condition (close-packed configuration)

The configuration is basically the same after the relaxation as figure 3.11. Figure 3.12 shows the time history of potential energy. From the figure 3.12, it is interesting to see that in this case the potential energy arrives at –92 arbitrary units, which is 24% lower than the first case. The results show that the atoms, with no constraints, try to move to the global minimum potential position as long as they have enough kinetic energy but they are restricted from their initial energy.

(c) Cubic model with periodic boundary condition

A third case is obtained by applying two-dimension periodic boundary conditions to the model for above case (a). Because of the symmetry and boundary condition, the

atoms cannot go anywhere to relax high potential energy. Thus, the configuration of atoms after relaxation is the same as in figure 3.7.

Figure 3.13 shows the time history of the potential energy. One can see that, the potential energy doesn't change at all, which demonstrates that the periodic boundary condition is a kind of 'kinematic constraint', so that some responses could be prevented. Comparing figures 3.10 and 3.13, the initial potential energy in figure 3.13 is higher because of more atoms taking part in the simulation actually and the property of periodic boundary condition itself.

Overall, as discussed in chapter 2.5, since a small number of atoms is used to simulate properties of material, choosing proper boundary conditions appreciably affects the correct numerical solution in the present algorithm.

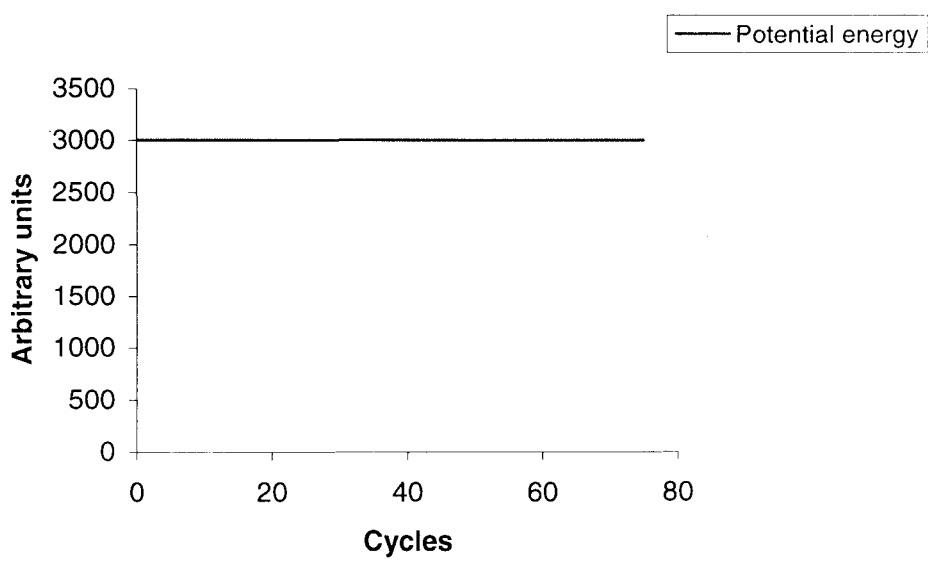

Figure 3.13 Potential energy as a function of simulation time for 2D model with two-dimension periodic boundary condition

3.3 Three-dimensional lattice

3.3.1 Model description

A three dimensional lattice is used to demonstrate effect of the different damping ratios on the equilibrium positions of the atoms. There are $5\times5\times5$ atoms arranged in the primitive cubic lattice as shown in figure 3.14. As done previously, the spacing between atoms is set to 0.8 arbitrary units and the cut-off radius is set to include two nearest neighbours. Both the Lennard-Jones pair potential energy function and changing mass algorithm are used. No boundary condition (free surface) is applied to the model.

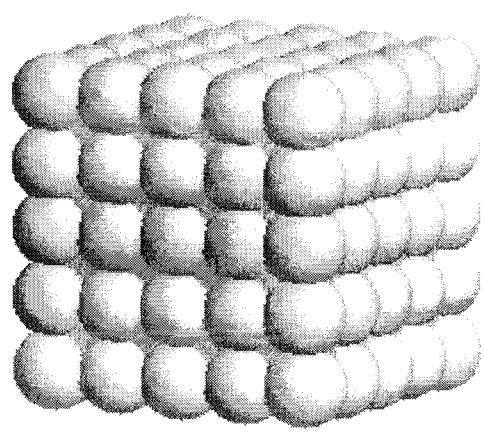

Figure 3.14 Initial configuration of three-dimensional lattice model

3.3.2 Tests and comparison

Six different damping ratios were tested in this model and their values were: 1.0, 2.0, 5.0, 10.0, 20.0 and 100.0 respectively. The test results are shown in table 3.1.

Damping ratio	Cycle numbers	Potential energy (Arbitrary units)
1.0	1845	-1329.5337
2.0	1075	-1367.3461
5.0	515	-1367.3461
10.0	390	-1332.6658
20.0	120	-947.2945
100.0	145	-947.2948

Table 3.1 Test results from three-dimensional lattice model

Compared to the other damping ratios (Table 3.1), when damping ratio equals 1.0, the system takes the longest time to converge because atoms could experience higher kinetic energy (high temperature) and become more active before stopping at equilibrium positions. As shown in figure 3.15, the cubic structure of the model is changed to an approximately spherical structure after the relaxation, which is explained by means of qualitative considerations. Figure 3.16 demonstrates the history of potential energy and kinetic energy, which shows more oscillations than when higher damping ratios are applied. However, this kind of result may not be the expected one.

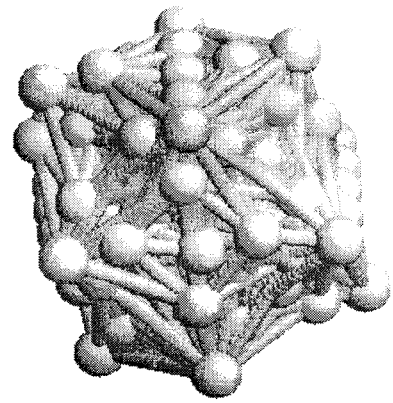

Figure 3.15 The configuration of 3D lattice model with damping ratio 1.0 after relaxation

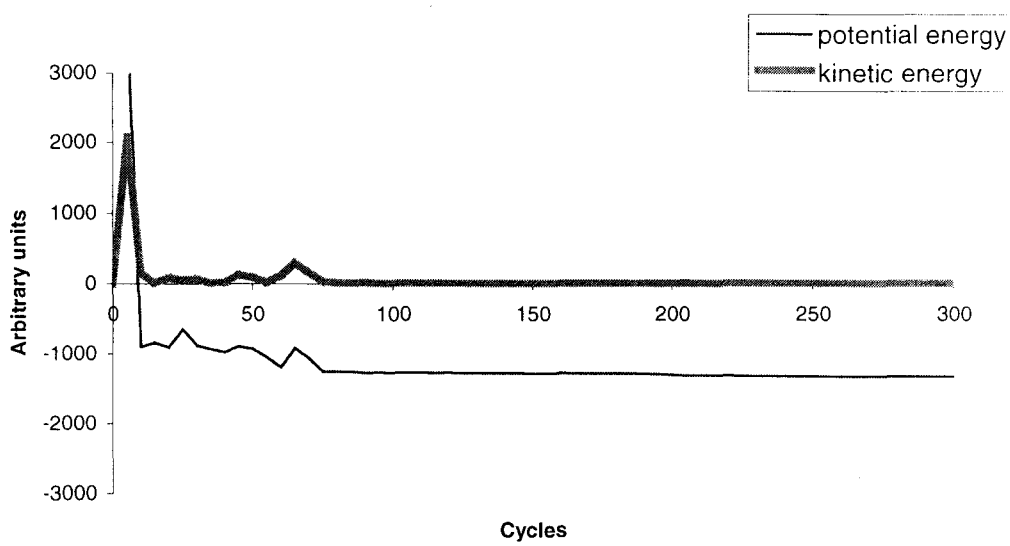

Figure 3.16 Potential energy and kinetic energy as a function of simulation time for 3D model with damping ratio 1.0

Figure 3.17 and figure 3.19 show the configuration after relaxation for which the damping ratio is set to 5.0 and 20.0 respectively. Figure 3.18 and figure 3.20 demonstrate the time history of potential energy and kinetic energy. When the damping ratio is 20.0, potential energy goes down to –947.3 arbitrary units, while the block of atoms just expands to its local equilibrium position and has not enough energy to go further. When the damping ratio is 5.0, it is of interest to see that the potential energy goes to -947.3 arbitrary units at first, and after staying at that level for some number of cycles, the high residual kinetic energy is able to push atoms to move closer to the global minimum potential energy state.

As mentioned in Chapter 2, the atomic movement to a new configuration is related to the maximum kinetic energy. Figure 3.21 shows that applying higher damping ratio like 20.0 makes the second maximum in kinetic energy disappear which prevents the system from moving further as when a damping ratio of 5.0 is chosen. Meanwhile, the maximum kinetic energy is higher when a lower damping ratio is chosen. Figure 3.22 (A and B) compares the two maximum kinetic energies for damping ratios of 2.0 and 5.0 respectively.

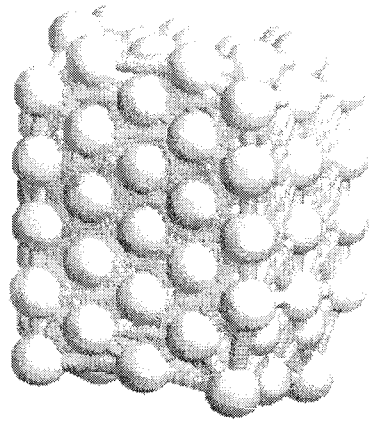

Figure 3.17 The configuration of 3D lattice model with damping ratio 5.0 after the relaxation

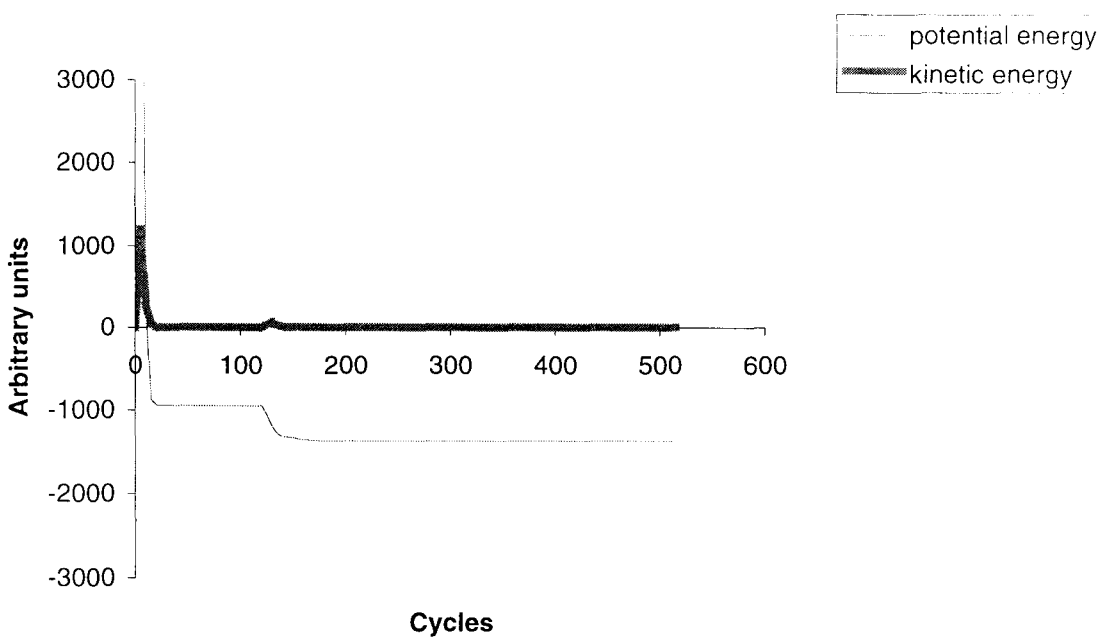

Figure 3.18 Potential energy and kinetic energy as a function of simulation time for 3D model with damping ratio 5.0

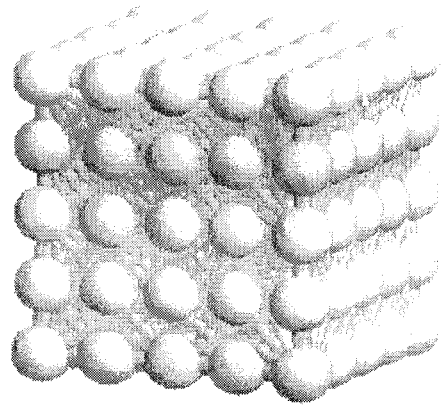

Figure 3.19 The configuration of 3D lattice model with damping ratio 20.0 after the relaxation

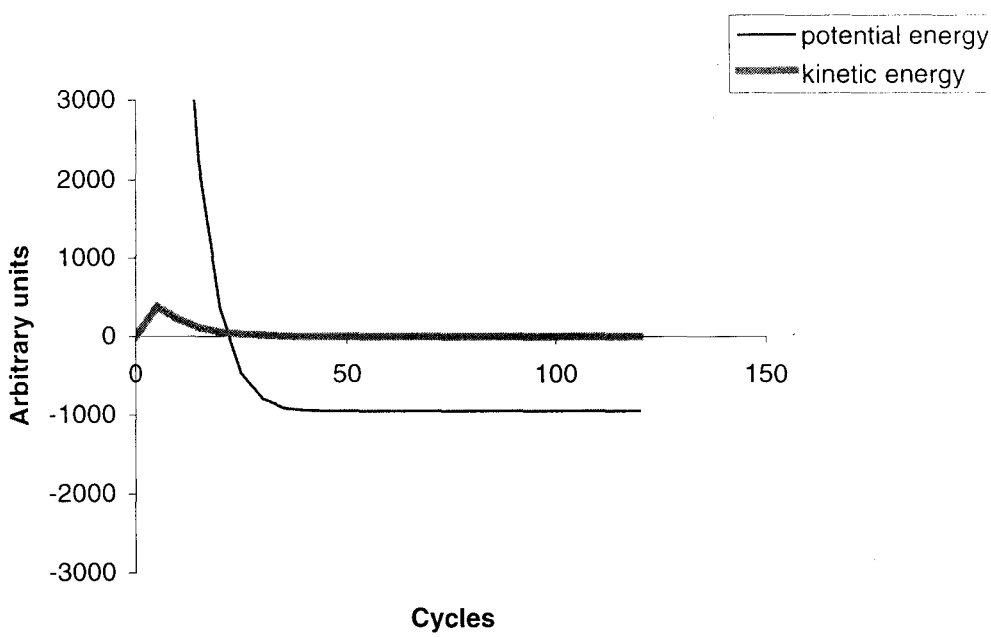

Figure 3.20 Potential energy and kinetic energy as a function of simulation time with damping ratio 20.0

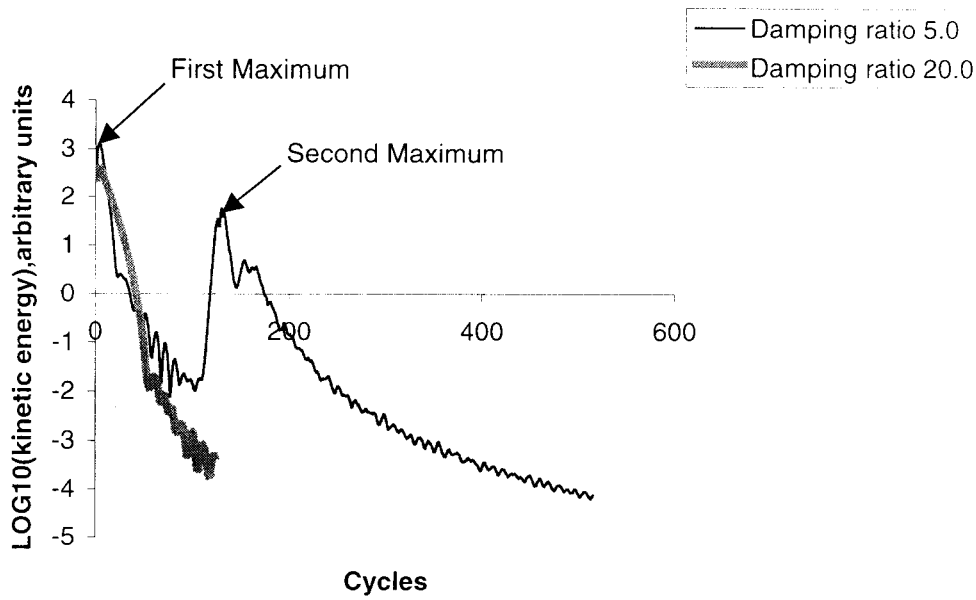

Figure 3.21 Kinetic energy as a function of simulation time of damping ratio 5.0 and 20.0

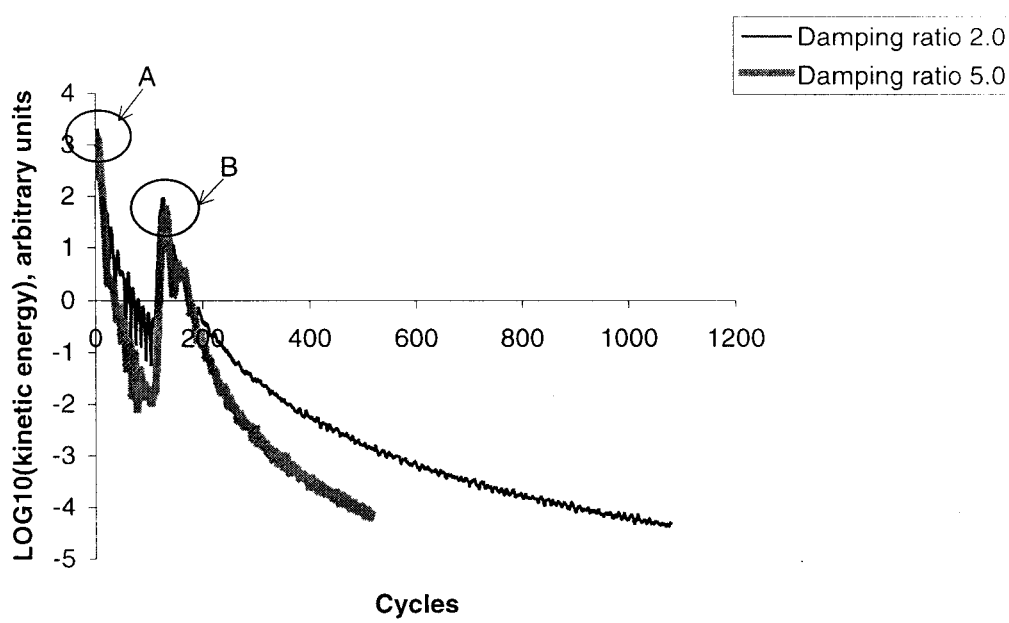

Figure 3.22 Kinetic energy as a function of simulation time of damping ratio 2.0 and 5.0

3.3.3 Discussion of damping effects

By testing different damping ratios as above in 3.3.2, the conclusion is made that the choice of damping ratio affects the response of the system in three ways:

(1) Convergence rate

The values of potential energy after relaxation are similar for a damping ratio 2.0 and 5.0. However, a damping ratio of 2.0 takes a longer time because atoms experience high kinetic energy so that they oscillate longer to the equilibrium position as seen in figure 3.22.

When the damping ratio is extremely high, i.e. 100.0, the minimum potential energy doesn't change much as it is observed for the damping ratio of 20.0, however, it consumes longer time to converge because of effect of over damping.

(2) Configuration

The total energy in the model is conserved. The differential potential energy transforms to kinetic energy in each step and is dissipated by damping step by step. The damping ratio determines how much kinetic energy is lost in the current step. Damping also affects the motion of atoms in next step to get new positions, on which the potential energy is dependent. So, the atoms could find positions where the potential energy is at the global minimum if a lower damping ratio is applied.

(3) Kinetic energy

Figure 3.21 and figure 3.22 shows that applying lower damping ratio causes the

system to experience higher kinetic energy (high temperature). This means that by applying a different damping ratio to the system, the kinetic energy (or temperature) can be altered during the simulation. Therefore, the damping ratio affects the solution path and different damping ratios may lead to different relaxation results.

3.4 Three-dimensional FCC lattice

3.4.1 Model description

A three dimensional FCC lattice is used to test properties of the lattice including an artificial edge dislocation, using EAM potential function.

Copper is used as a test material and relevant parameters for simulation are obtained from Ackland *et al.*[10] and are given in Chapter 1. Initially, 172 atoms are generated in the perfect FCC lattice (figure 3.23). By removing a certain half plane, an artificial edge dislocation is introduced along Y direction to the test model (figure 3.24). During the simulation, the mass is fixed and damping ratio is set to 20.0.

3.4.2 Tests and comparison

Two tests are presented here. One is a free body and the other test is with a periodic boundary condition along the dislocation line direction (Y axis).

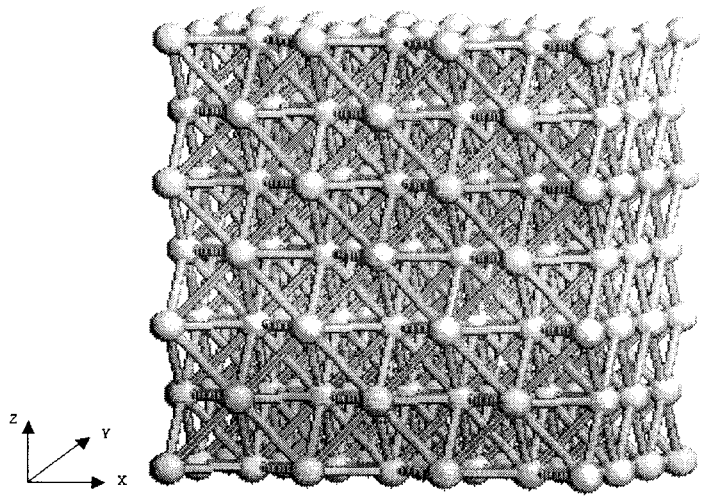

Figure 3.23 Perfect FCC lattice model

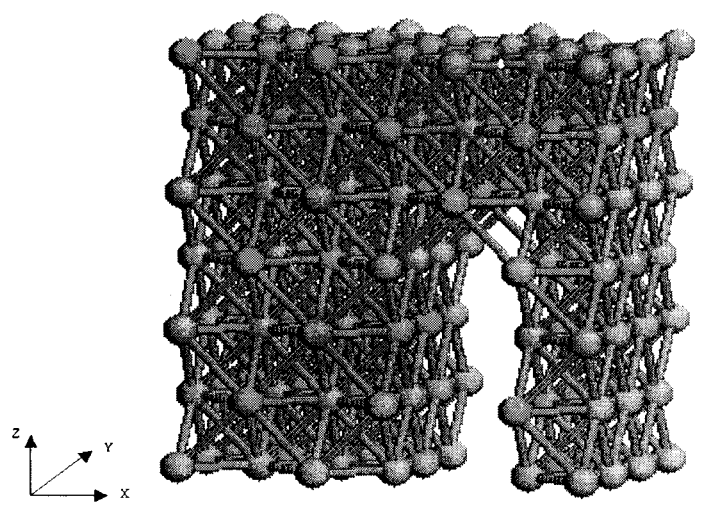

Figure 3.24 FCC lattice model with an edge dislocation

Simulation results presented in figure 3.25 to figure 3.28 are in agreement with the qualitative consideration within the framework of the dislocation theory. Due to the free boundary condition and lack of neighbours, the atoms at the corner of the block are more active than atoms in the other part of the block. As observed in figure 3.25 (A), the atom at the corner jumps to the other layer. This phenomenon disappears after applying periodic boundary conditions to the model.

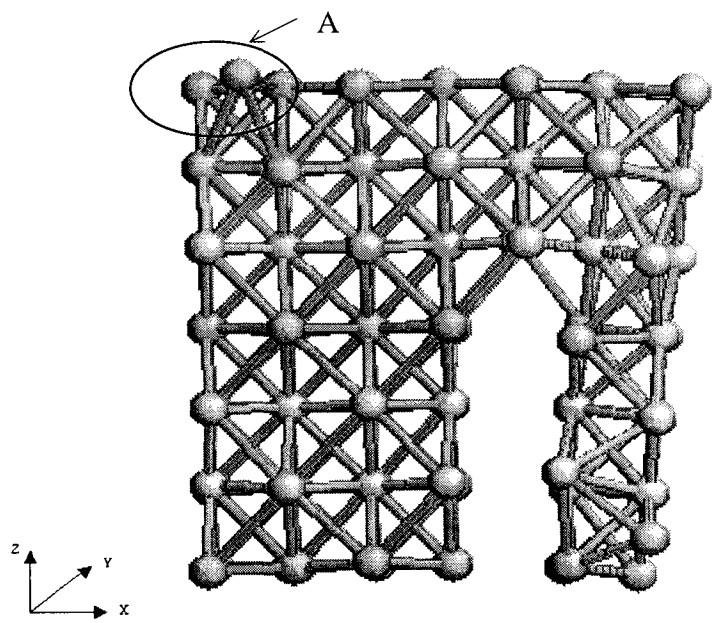

Figure 3.25 The configuration of 3D f.c.c. model with dislocation after relaxation (free body)

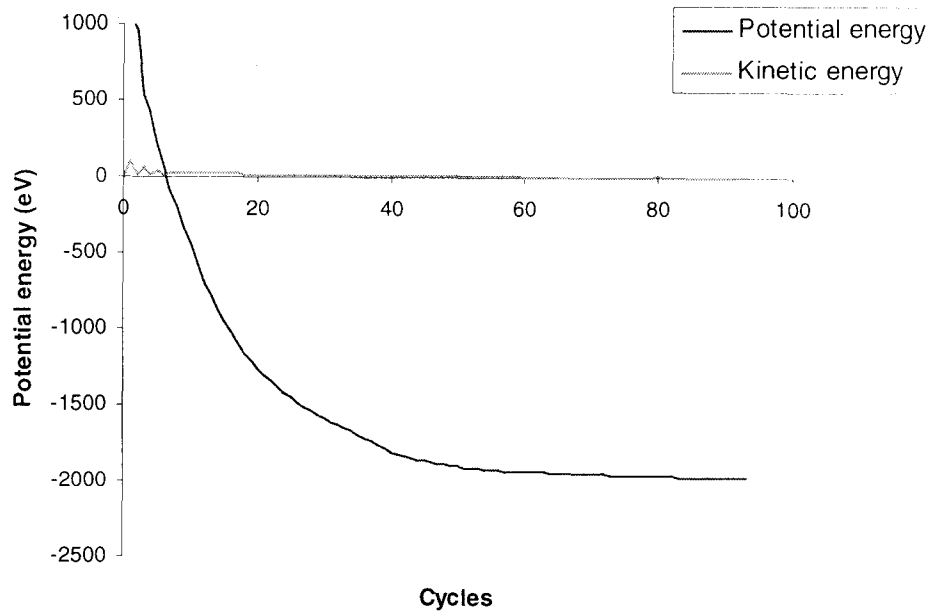

Figure 3.26 Potential energy and kinetic energy as a function of simulation time for 3D f.c.c. model with a dislocation (free body)

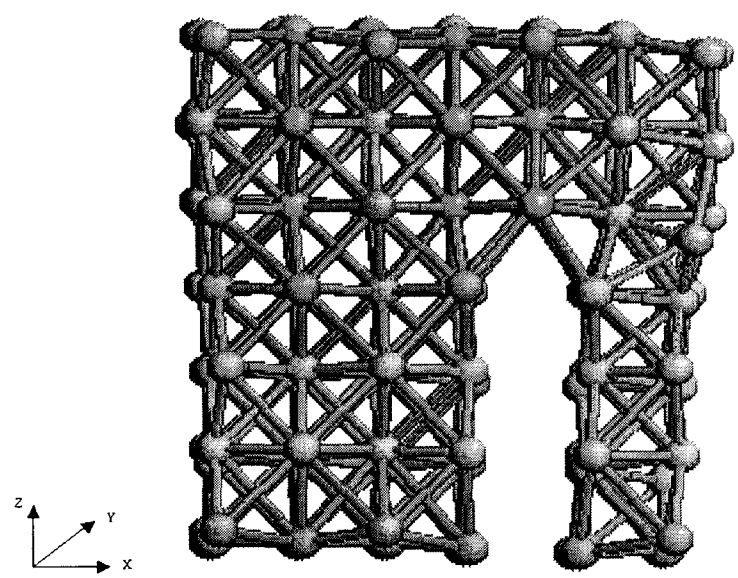

Figure 3.27 The configuration of 3D f.c.c. model with dislocation after relaxation (periodic boundary condition along Y axis—dislocation line)

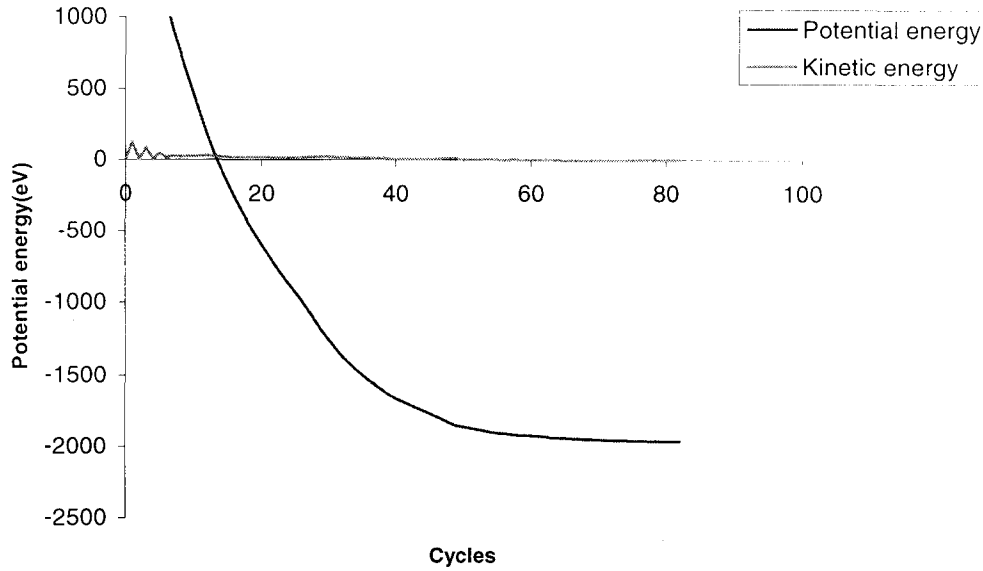

Figure 3.28 Potential energy and kinetic energy as a function of simulation time for 3D f.c.c. model with a dislocation (periodic boundary condition along Y axis)

3.4.3 Discussion of using EAM potential

(1) When the damping ratio value is set to 1.0 or lower, it is found that the block of atoms cannot keep its shape, or even splits into several pieces. This means that the extremely low damping ratio is not suitable to the model under the EAM potential energy function. When applying much lower damping ratios to the system, from the Dynamic Relaxation algorithm itself, large displacements for the atoms in every time step are possible. Since potential energy functions are sensitive to the positions of atoms, sufficiently large displacements could be beyond the allowable range for the EAM potential energy function so that the block of atoms breaks or explodes. Therefore, a higher damping ratio

is recommended for the calculations using EAM potential energy function.

(2) While simulating a perfect 3D f.c.c. lattice (figure 3.23), in order to get relaxation result under the EAM potential energy function, it was expected that the shape of whole block of atoms does not change i.e. the lattice parameter remains at the value $3.615\,\mathring{A}$. However, the present result shows that the lattice parameter expands 16% - 17%. From the view of Dynamic Relaxation algorithm, there is internal stress existing in the perfect 3D f.c.c. lattice using parameters from Ackland *et al*[10]. Because of the pre-existing internal stress, there is a trend to expand the model during the simulation. As a result, the change of the configuration now does not all come from internal defects; On the other hand, if applying certain boundary conditions, part of the residual stress after the simulation may come from the pre-existing internal stress.

(3) An interesting observation experienced during the simulation is that the block of atoms is moving during the relaxation (figure 3.29). As mentioned by Voter[5], this is the 'defect' feature of EAM method, which leads to a displacement of a whole block of atoms as they seek new equilibrium positions. The EAM potential at one atom is the summation of pair potential ($\sum_j V_{ij}$) due to pairwise interactions plus a correction function ($f(\rho_i)$). The correction function is dependent on the number of atomic neighbours. Because of this, the forces from the correction function cannot be balanced. So that, the net force in the model is not zero and pushes the model to move. Although the net force

is small compared to the interactions, it still violates the basic principle of systems of particles, which states that the resultant internal force should be zero.

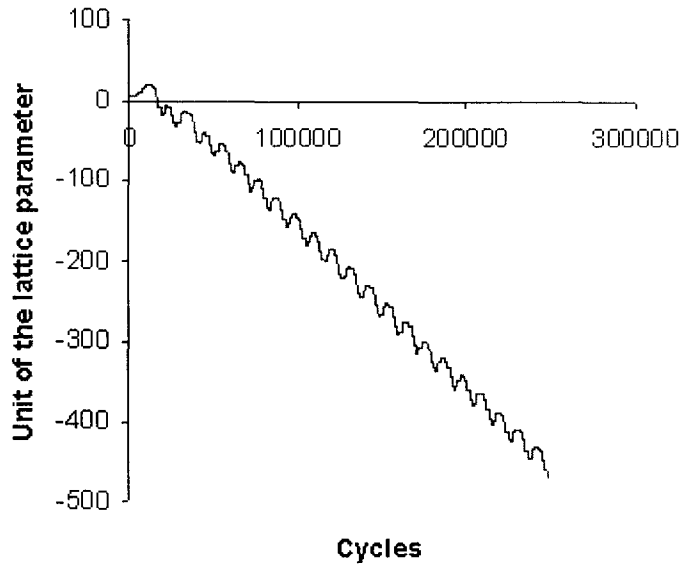

Figure 3.29 X coordinate of certain atom as a function of cycles

Kinematic boundary conditions i.e. fixed or periodic boundaries can hide this feature, but the corresponding reaction should be larger than expected at the boundary. The solution could be to apply the extra force and moment to balance the system, which is inconvenient using the present approach. Alternatively, the EAM potential is often transformed to the effective pair potential function, which will fix the problem and also simplify the calculation.

CHAPTER 4 – RELAXATION OF THREE-DIMENSIONAL FCC LATTICE WITH A DISLOCATION

This chapter presents modified Dynamic Relaxation technique to simulate the relaxation of a real material model with a dislocation. The comparison between the new Dynamic Relaxation algorithm and existing software for simulating dislocation core structure is discussed.

4.1 Model Description

The material model used in this exercise was generated by the external lattice creator software[28]. The model consists of 5055 atoms in the shape of three-dimensional disk (figure 4.1, X-Y top plane). A 60 degree dislocation was introduced to the block of atoms using anisotropic elasticity theory (figure 4.2). The dislocation line is along Z direction. The material is copper and the relevant parameters are under EAM potential energy function. The cut-off distance used was to cover third nearest neighbors.

In describing the crystallographic orientation of the model, it is customary to use coordinate system such that: **X**=[2 –1 1], **Y**=[1 1 -1], **Z**=[0 1 1]. The results of displacement and final configuration of atoms are defined in this system.

The requirement for the boundary condition is that: (i) all the atoms at the physical boundary of the model are fixed in X and Y directions, and (ii) in Z direction, periodic

boundary condition is applied to all the atoms of the model.

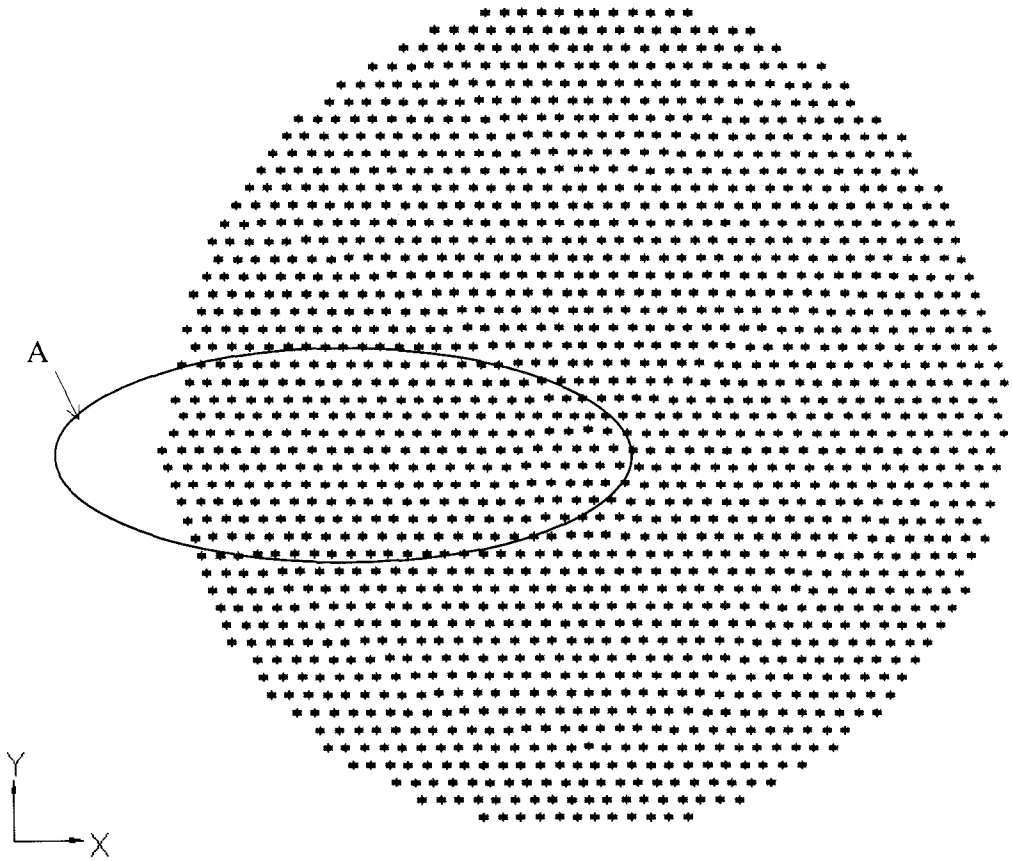

Figure 4.1 Atomistic model of three-dimensional fcc lattice in form of a cylinder (disk) with a dislocation in the area at A, X-Y is the top plane of the cylindrical lattice (disk)

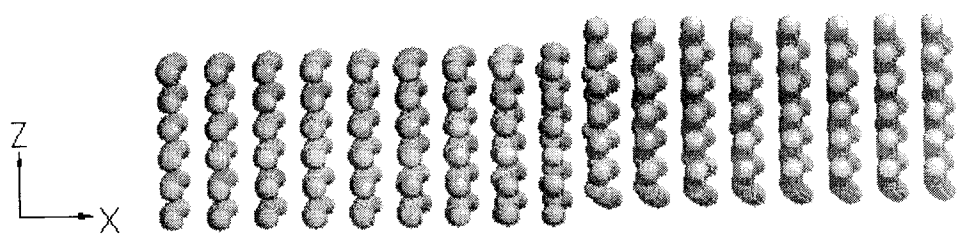

Figure 4.2 Enlarged part of the dislocation in figure 4.1 A (Z-Y plane)

4.2 Technical Details

4.2.1 Boundary condition in X and Y directions

Rather than for the cubic shape of the model, an uneven distribution of the atoms at the physical boundary in the present case makes it difficult to locate the atoms at the boundary. The approach for locating the atoms at the circular boundary is thus different from the cubic model. The method of fixing atoms at the physical boundary in X and Y direction in this model is as follow:

(1) Since the origin locates the center of the circular plate, the radius r of the circle can be determined by

$$r = \frac{Min(D_x, D_y)}{2} \tag{4.1}$$

Here D_x and D_y are maximum distance in X and Y direction respectively.

(2) Suppose the coordinate of any atom i is (x_i, y_i, z_i), if the values of x_i and y_i satisfy any one of the following two inequalities

$$\left|\sqrt{x_i^2 + y_i^2} - r\right| < r_{tol} \tag{4.2}$$

$$\sqrt{x_i^2 + y_i^2} > r \tag{4.3}$$

where r_{tol} is a tolerance value, the atom is treated as the boundary node.

(3) If the value of r_{tol} is small, a thin ring of boundary atoms can be obtained (figure 4.3). Then the boundary atoms are fixed at X and Y direction. However, the restriction is just

for the boundary atoms themselves, not for the boundary ring. Therefore, in some areas where the seams between atoms are large enough like figure 4.3 A, B and C, the internal atoms could escape from the seams (figure 4.4). The solution to this problem is to increase the thickness of the boundary ring (figure 4.5), i.e. enlarging the value of r_{tol}. Since the dislocation is located in the middle of the model, the relaxation of the lattice will occur around that area, which slightly affect atoms near the physical boundary. Therefore, increasing the number of boundary atoms is a practical way to stabilize the simulation.

4.2.2 Periodic boundary condition in Z direction

The arrangement of atoms in Z direction is shown in figure 4.6. The primitive length in Z direction cannot be calculated as described in the chapter 2.5.1, i.e. the distance is between top atom A and bottom atom C, which is 2.5 times of unit length D1. This is because atom A and its image atom B lose their uniform motion under the periodic length of $2.5 \times \mathrm{D1}$. The reason for this is that the periodic distance should not be the fractionary multiples of unit length D1.

For the configuration in this model, the primitive length in Z direction also could not be adjusted to D2, which is two times of unit length D1. At this stage, the cut-off distance r_c is larger than half the length of primitive length D2 ($\mathrm{D1} < r_c < \mathrm{D2}$), which violates the rule of periodic boundary condition defined in chapter 2.5.1.

In this particular model, an alternative solution for the above problem is to change

the primitive cell and increase periodic length to three times of unit length D1, as D3 shown in figure 4.6. Using D3 as periodic length in Z direction ensures the atoms and their images have uniform motion and the treatment is used in the source code for the model.

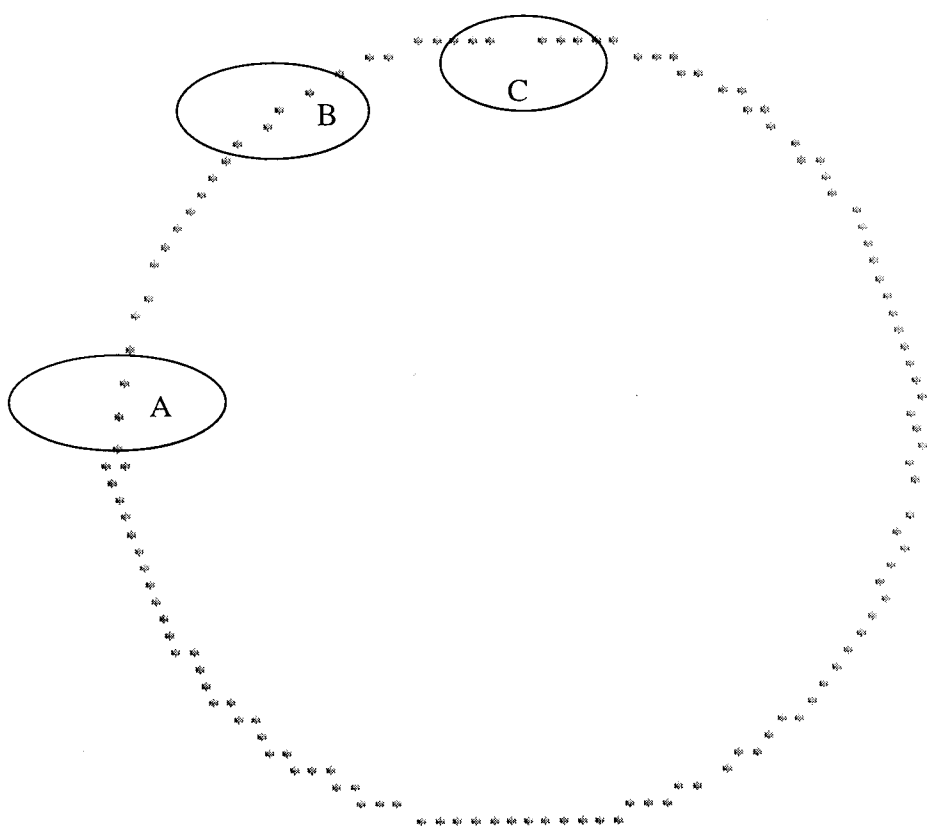

Figure 4.3 Boundary atoms with small r_{tol} value

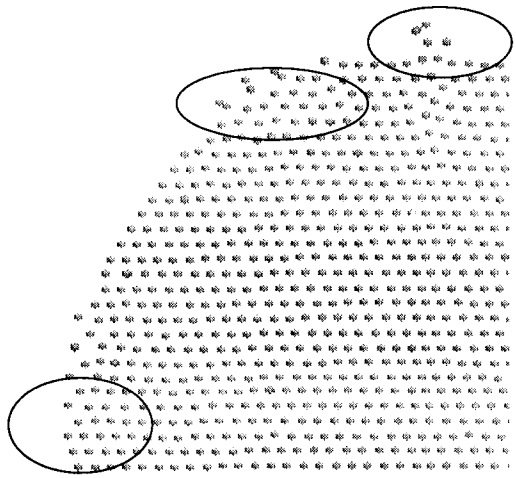

Figure 4.4 Part of the lattice with the positions of internal atoms which escape from the seams

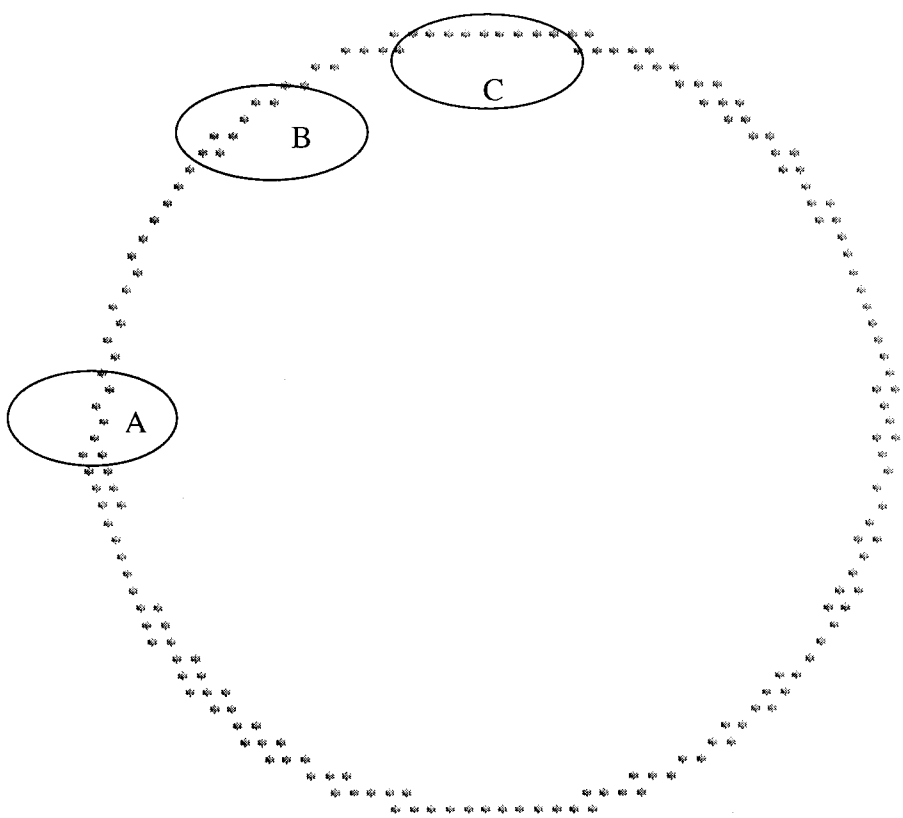

Figure 4.5 Structure of boundary atoms with large r_{tol} value

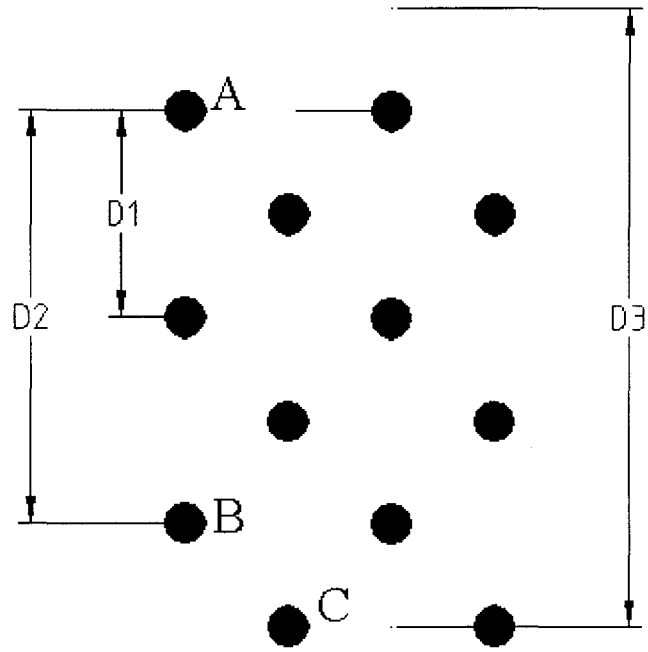

Figure 4.6 Scheme of atom configurations in Z direction

4.2.3 Damping Ratios and Tolerance

Since there are many atoms involved in the simulation, inequality (2.51) is chosen as the convergence criterion and the tolerance number f_{tol} is set as 0.01.

As mentioned in Chapter 3.3.2, different damping ratios could lead to different relaxation results. Figures 4.7 and 4.8 presents histories of potential energy and kinetic energy with different damping ratios of 2.0, 10.0, 20.0, and 50.0. The results show there are two kinds of responses of the model when applying higher damping ratios e.g. 20.0 or 50.0 and lower damping ratios e.g. 2.0 or 10.0 into the model.

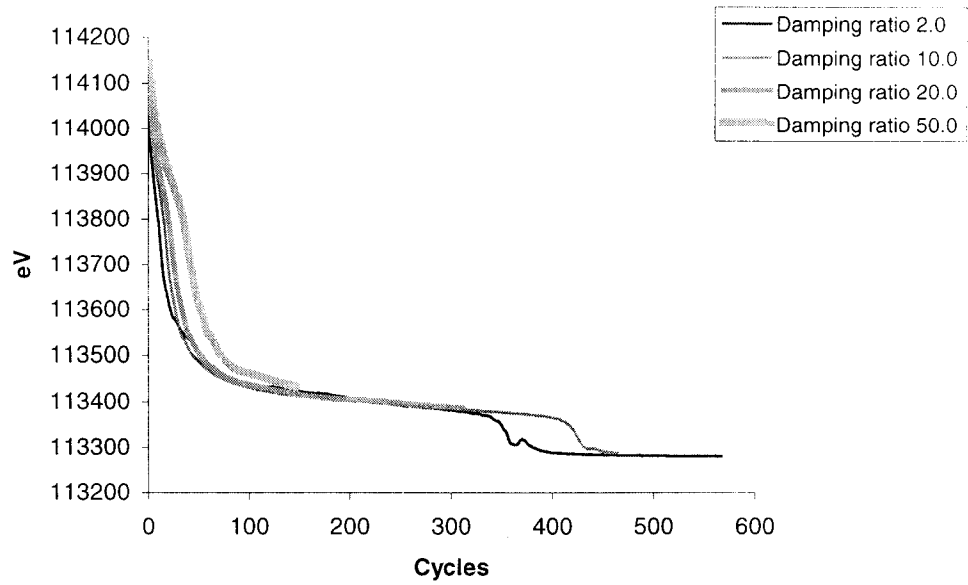

Figure 4.7 Potential energy as a function of simulation time with different damping ratio (stopped at the same tolerance value)

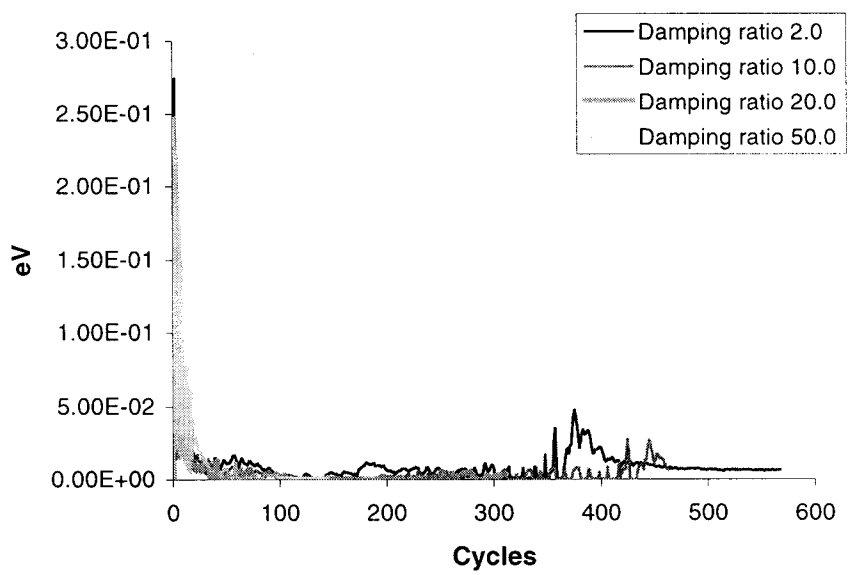

Figure 4.8 Kinetic energy as a function of simulation time with different damping ratio (stopped at the same tolerance value)

4.3 Results and Comparison

The computer used for the calculation was general personal computer with Pentium 550 MHz CPU.

The Molecular Dynamics (MD) software[29] was also used to simulate relaxation of the same model as above in order to compare the results with the approach used in the literature [29] and new Dynamic Relaxation approach.

The visual tool for representing the results and comparison of two techniques is the software Disregistry[30]. Disregistry chooses one line of atoms around dislocation area and then calculates relative displacements based on their current positions in the defect lattice with respect to the positions in the perfect lattice. The relative displacement is decomposed into screw dislocation component and edge dislocation component.

Figures 4.9 and 4.10 show the screw and the edge component for the initial configuration model with the 60 degree dislocation at the center of the model (figure 4.1).

4.3.1 Higher damping ratios

Figure 4.11 and figure 4.12 show the relaxation results for (i) damping ratio 20.0, (ii) damping ratio 30.0, (iii) damping ratio 50.0 and (iv) Molecular Dynamics software[29].

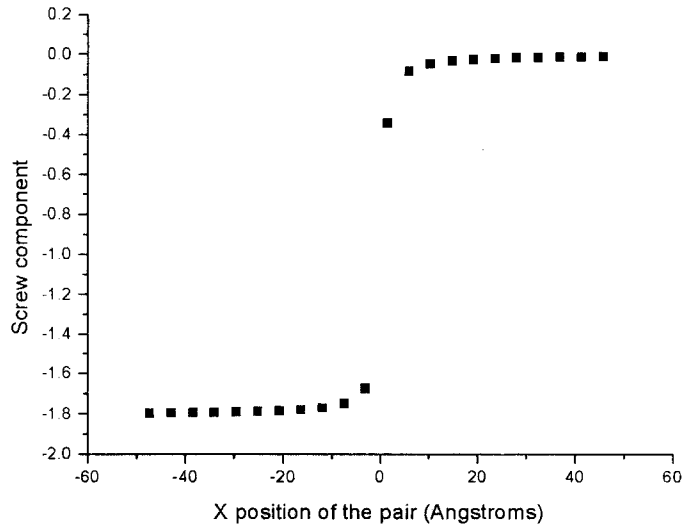

Figure 4.9 Screw component of a Burgers vector of dislocation in the initial model determined by Disregistry

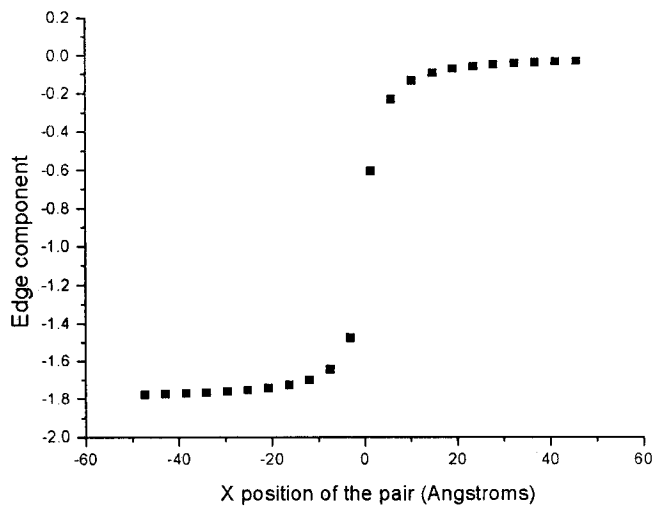

Figure 4.10 Edge component of a Burgers vector of dislocation in the initial model determined by Disregistry

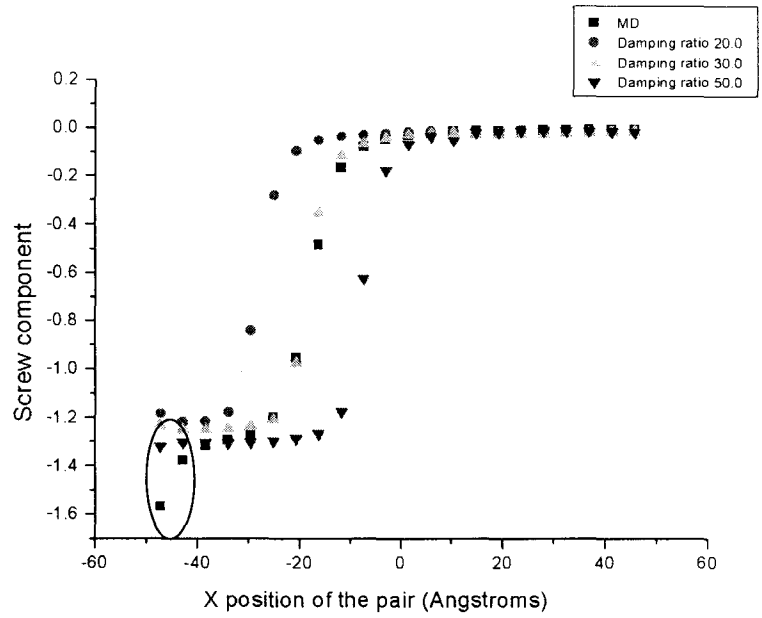

Figure 4.11 Comparison of screw component of a Burgers vector of dislocation for various damping ratios

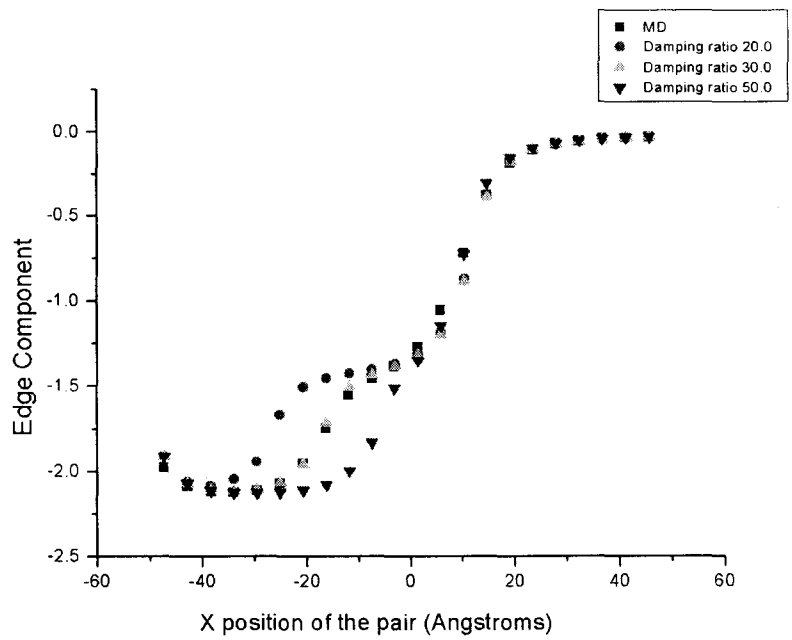

Figure 4.12 Comparison of edge component of a Burgers vector of dislocation for various damping ratios

The model was tested initially by using the damping ratio of 20.0 and 50.0. It is of interest to see from the figure 4.11 and figure 4.12 that the results of MD simulation are located in the middle of DR results for damping ratio 20.0 and 50.0 and all of them have the some trend. It is apparent that for the damping ratio of 30.0 the result of DR matches these of MD very well, except the boundary atoms (circle area in figure 4.11). The reason of this discrepancy is that different boundary treatments are used in these two approaches. Moreover, because MD uses different kind of EAM potential energy function and different numerical integration of the equation of motion from DR method, these two approaches are expected to generate slightly different solutions.

4.3.2 Lower damping ratios

Figure 4.13 and figure 4.14 compare the results of DR algorithm with: (i) damping ratio of 2.0 (ii) damping ratio of 10.0 and with an initial configuration of the dislocation.

When applying a lower damping ratio into the model, atoms can experience higher kinetic energy (temperature). Therefore, system has a tendency to get rid of a dislocation and restore the perfect lattice. From the figure 4.13 and figure 4.14, atoms almost loose the screw component (Z direction). However, due to the strong restriction in the X and Y direction, the edge component of a dislocation cannot be totally eliminated and remains in the model.

Another interesting feature of the Dynamic Relaxation response is the motion of the

Burgers vector during the simulation. Figures 4.15 and 4.16 show how the Burgers vector moves through other equilibrium positions using damping ratio 2.0. Therefore, damping ratio could control equilibrium shapes of the model.

4.3.3 Summary

The solution for the real material model proves that the damping ratio is the key parameter of Dynamic Relaxation techniques when applied to the atomistic simulations. The configuration tested in chapter 4.3.2 shows that Dynamic Relaxation could be an alternative tool for atomistic simulation or can be used to as an independent check of the validity of different Molecular Dynamics softwares.

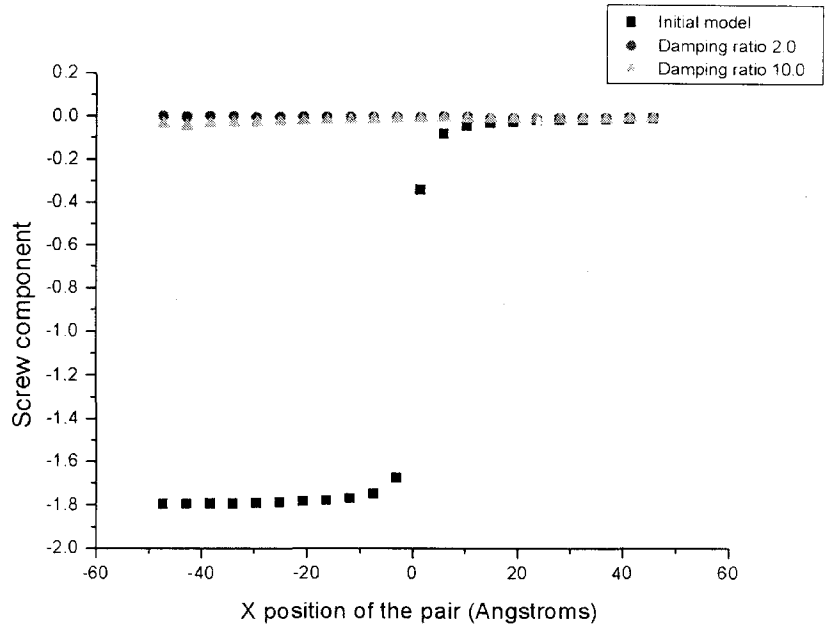

Figure 4.13 Comparison of screw component of a Burgers vector of dislocation for lower damping ratios

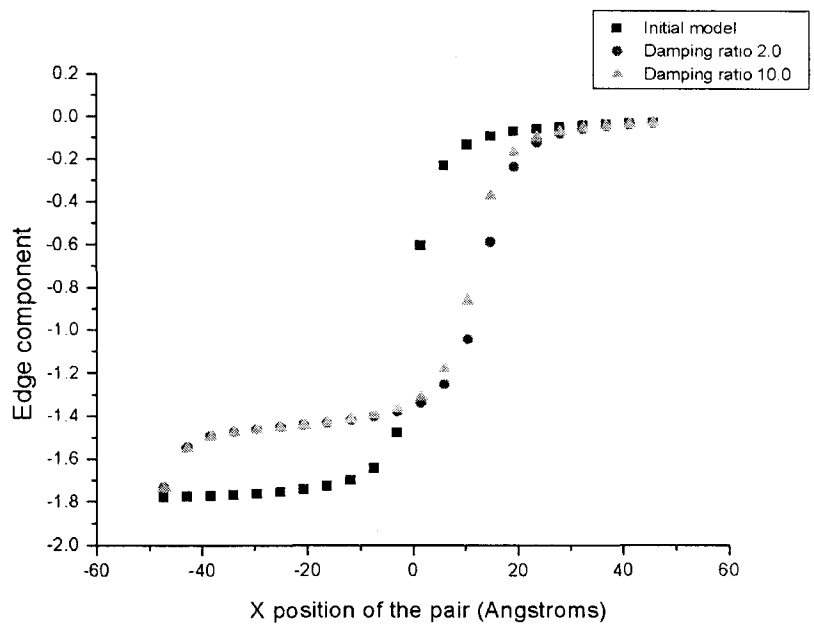

Figure 4.14 Comparison of edge component of a Burgers vector of dislocation for lower damping ratios

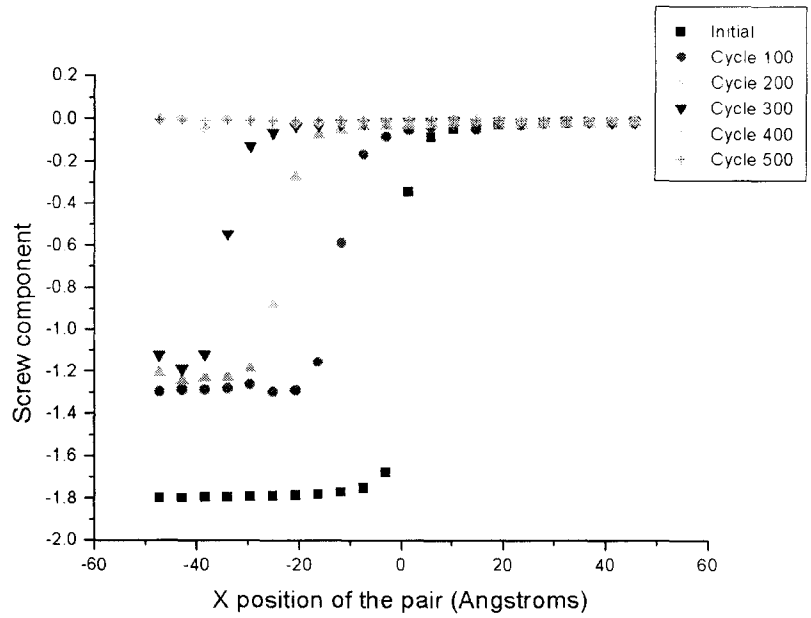

Figure 4.15 Comparison of screw component of Burgers vector of dislocation for various simulation time (damping ratio 2.0)

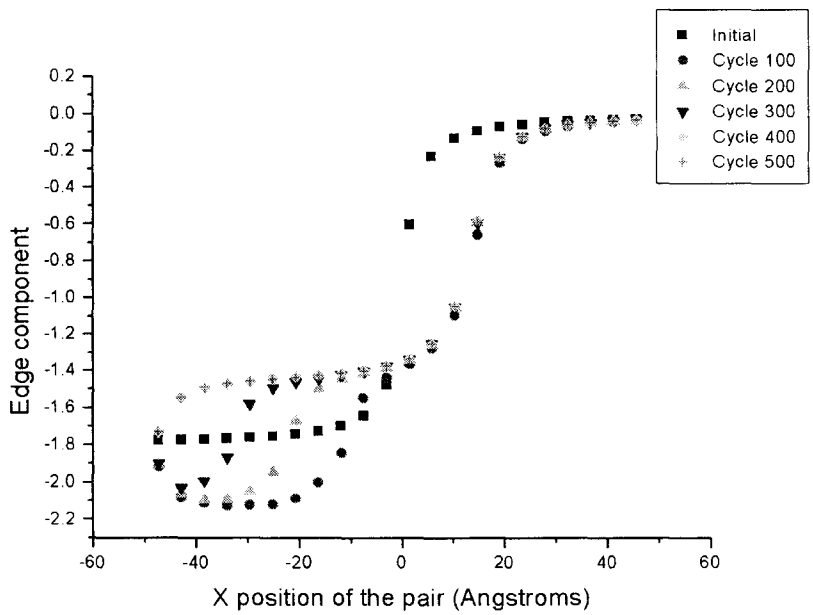

Figure 4.16 Comparison of edge component of Burgers vector of dislocation for various simulation time (damping ratio 2.0)

CHAPTER 5 – CONCLUSION AND RECOMMENDATIONS

5.1 Conclusion

The present work deals with the development of new algorithm based on Dynamic Relaxation technique to simulate molecular structure of crystalline material. The use of Dynamic relaxation techniques in molecular simulations is thus a new application of Dynamic Relaxation techniques itself and gives researchers in material science or other scientific disciplines some possibilities to study the properties of materials.

Dynamic Relaxation, a powerful tool for non-linear mechanical problems, has also shown its promising future for simulation of the atomic structure of materials. Internal force and stiffness are obtained as derivatives of potential energy function and this is required modification of Dynamic Relaxation techniques to be used in conjunction with the meshless Finite Element Analysis.

From the all tests carried out so far, the convergent solution for the atoms can always be obtained using modified Dynamic Relaxation algorithm. Different equilibrium shapes are obtained by adjusting the damping ratio, which is the major difference from continuum approach. Using Dynamic Relaxation for simulating practical material model, one can obtain very similar results as these using existing Molecular Dynamics software.

The periodic boundary condition, which is not often used in continuum Finite Element Analysis, was thoroughly studied and successfully implemented into the simulation.

5.2 Recommendations

The future work will include such aspects as:

(1) Studying of accelerating convergence for the simulation, in which the participating frequency of the overall model is much lower than the highest frequency of the model. More accurate stiffness estimation is a possible way to solve the problem.

(2) Studying the numerical response when applying external force, e.g. cutting force, on the model, which could explain some phenomena in the metal implements.

(3) Implementing contact algorithm to surface atoms and physical boundary for connecting atomistic simulation and continuum simulation, e.g. fracture problem.

(4) On the material side, the interaction between defects and how they affect the material properties can also be studied.

Reference

[1] Frenkel, D. and Smit, B., 1996, "Understanding molecular simulation: from algorithms to application," Academic Press, Inc

[2] Ercolessi, F., 1997, "A molecular dynamics primer," ebook, http://www.fisica.uniud.it/~ercolessi/md/md, 1997

[3] Bullough, R., and Tewary, V. K., 1979, "Lattice Theories of Dislocations," *Dislocations in Solid*, Vol. 2, pp. 41-62

[4] Daw, M. S. and Baskes, M. I., 1984, "Embedded-atom method: Derivation and application to impurities, surfaces, and other defects in metals" *Physical Review B*, Vol. 29, No. 12, pp. 6443-6453

[5] Voter, A. F., 1994, "The Embedded-Atom Method" *Intermetallic Compounds*, Vol.1, Principles, pp. 77-90

[6] Harrison, W. A., 1966, "Pseudopotential in the theory of Metals," *Benjamin*, New York.

[7] Finnis, M. W. and Sinclair, J. E., 1984, "A simple empirical N-body potential for transition metals" *Philosophical Magazine A*, Vol. 50, No. 1, pp. 45-55

[8] Masuda, K., and Sato, A., 1981, *Phil. Mag.* A, **44**, 799

[9] Kogure, Y., and Kosugi, T., 1996, "Simulation of Dislocation Dynamics in FCC Metals" *JOUENAL DE PHYSIQUE IV*, Vol. 6, Colloque C8, pp. 195-198

[10] Ackland, G. J., Tichy, G., Vitek, V. and Finnis, M. W., 1987, "Simple N-body potentials for the noble metals and nickel" *Philosophical Magazine A*, Vol. 56, No. 6, pp. 735-756

[11] Christensen, N. E. and Heine, V., 1985, *Phys. Rev.* B, **32**, 6145

[12] CSEP, 1995, " Introduction to Monte Carlo Methods," ebook, http://csep1.phy.ornl.gov/mc/, 1995

[13] B. J. Alder and T. E. Wainwright, 1957, *J. Chem. Phys.* 27, 1208

[14] Press, W. H., Teukolsky, S. A., Vetterline, W. T. and Flannery, B. P., 1992, "Numerical Recipes in FORTRAN: The art of Scientific Computing ", 2nd Ed, Cambridge: Cambridge University Press

[15] Cook, R. D., Malkus, D. S. and Plesha, M. E., "Concepts and applications of finite element analysis", Third edition, John Wiley & Sons, 1989

[16] A. S. Day, 1965, "An Introduction to Dynamic Relaxation," *Engr, Lond.*, **219**, 218-221

[17] Brew, J.S., and Brotton, D. M., 1971, "Non-Linear structural analysis by Dynamic Relaxation," *International Journal Numerical of Methods in Engineering*, Vol. 3, pp.436-483

[18] Pica, A., and Hinton E., 1980, "Transient and Pseudo-Transient Analysis of Mindlin Plates," *International Journal of Numerical Methods in Engineering*, Vol.15 , pp.189-208

[19] Kant, T., and Patel, S., 1990, "Transient/Pseudo-Transient Finite Element Small / Large Deformation Analysis of Two-Dimensional Problems," *Computers and Structures*, Vol. 36, No. 3, pp. 421-427

[20] Underwood, P., 1983, "Dynamic Relaxation," *Computational Methods for Transient Analysis*, Vol.1, pp. 245-265

[21] Sauvé, R. G., and Metzter, D. R., 1995, "Advances in Dynamic Relaxation

Techniques for Nonlinear Finite Element Analysis," *Transactions of the ASME*, Vol. 117, pp. 170-176

[22] Belytschko, T,. 1983, "An overview of Semidiscretization and time integration procedures," *Computational Methods for Transient Analysis*, eds., T. Belytschko and T. J. R. Hughes, North Holland, pp. 1-66

[23] Cook, R. D., "Finite element modeling for stress analysis," John Wiley $ Sons, 1994

[24] Sands, D. E., "Introduction to crystallography," Dover Publications, Inc., 1993

[25] Nobel, B., "Applied Linear Algebra," Prentice-Hall, Inc., 1969

[26] The MathWorks Inc, "Matlab", software, Version 5.3.0-10183 (R11), 1999

[27] Waterloo Maple Inc, "Maple", software, Version 4.00a, 1996

[28] Daw, M. S. and Foiles, M., "Lattice Creator", software, 1994

[29] Hoagland, R. G., "Molecular Dynamics", software, 1998

[30] Hoagland, R. G., "Disregistry", software, 1998

[31] Sayle, R., "Rasmol", software, 1999

[32] Sauve, R. G., "H3DMAP Version 6.0 – A General Three Dimensional Finite Element Computer Code for Linear and Nonlinear Analysis of Structures," Ontario Power Technologies Report No. A-NSG-96-120, Rev. 1, 1999

[33] Weertman, J. and Weertman, J. R., "Elementary Dislocation Theory," The Macmillan Company, 1964

[34] Avner, S. H., "Introduction to Physical Metallurgy", Second Edition, McGRAW-HILL Book Company, 1974

[35] Belytschko, T., Liu, W. K. and Moran, B., "Nonlinear Finite Element for Continua

and structures," John Wiley & Sons, LTD, 2001

[36] Smith, I. M. and Griffiths, D. V., " Programming the Finite Element Method," Third edition, John Wiley & Sons, LTD, 1997

[37] Hoagland, R. G., Mitchell, T. E., Hirth, J. P. and Kung, H., 2002, "On the strengthening effects of interfaces in multiplayer fcc metallic composites," *Philosophical Magazine A*, Vol. 82, pp. 643-664

[38] Miller, R. Tadmor, E. B., Phillips, R. and Ortiz, M., 1998, "Quasicontinuum simulation of fracture at the atomic scale," *Modelling simulation material science engineering*, 6, pp. 607-638

[39] Pawaskar, D. N., Miller, R. and Phillips, R., 2001, "Structure and energetics of long period tilt grain boundaries using an effective Hamiltonian," Physical Review B, Vol. 63, pp. 214105-1 – 214105-14

[40] Yasin, H., Zbib, H. M. and Khaleel M. A., 2001, "Size and boundary effects in discrete dislocation dynamics: coupling with continuum finite element," *Matericals Science and Engineering*, A 309-310, pp. 294-299

[41] Kamerich, E. and translated by Tang, J. and Li., J, "Introduction to Maple," China Higher Education press Beijing and Springer-Verlag Berlin Heidellberg, 2000

[42] Dyck, V., Lawson, J. D., and Smith, J. A. "Fortran / 77: An Introduction to Structured Problem Solving," Reston Publishing Company, Inc. and A Prentice Hall Company, 1984

[43] Chapra, S. C. and Canale, R. P., "Numerical Methods for Engineers with Programming and Software Application," Third Edition, WCB / McGraw-Hill, 1998